

DRILL STRING AXIAL VIBRATION AND SONIC
HEAD ANALYSIS

KAMBIZ EMTEHANI JAHROMI



DRILL STRING AXIAL VIBRATION AND SONIC HEAD ANALYSIS

by

© Kambiz Emtehani Jahromi

A Thesis submitted to the

School of Graduate Studies

in partial fulfillment of the requirements for the degree of

Master of Engineering

Faculty of Engineering and Applied Science

Memorial University of Newfoundland

April 2012

St. John's

Newfoundland

ABSTRACT

This study contains several analyses about vibration generation devices and axial vibration in the drill string. Advanced Drilling Group (ADG) has been seeking new technologies in drilling to improve the rate of penetration (ROP), and in this regard several vibration generation devices for rotary drilling have been reviewed for further analysis. The Sonic Head Drill (SHD) is one of the most prominent drilling tools in shallow depth drilling, and is the focus of the first part of this study. This study attempts to determine if this tool can be used for laboratory and field tests, and if the concept of unbalanced masses used in the SHD can be successful in oil and gas drilling. In order to determine the feasibility and ease of use of the SHD, a series of tests and simulations were conducted in this thesis. A sonic head is surrounded by four isolators. These isolators are experimentally characterized and the force transmitted to the rock and the frame is predicted. Several other vibratory systems were also reviewed and a basic model of a vibratory system based on the SHD principle is proposed. The vibration generation device designed is 127 mm (5 inches) in diameter and 0.5 m long. It can generate 74.5 kN vibratory force at the frequency of 150 Hz compared to 100 kN for the SHD. The drill string transfers rotary and vibratory motion to a drill bit. Drill string vibration is a very prevalent phenomenon; it has a great effect on drilling engineering, and drill string resonance is the main reason causing drill string fatigue. The drill string is connected to the vibration generation device proposed in this study, and it is another purpose of this study to analyze the effect of vibration on the drill string. Possible solutions are explored

on how a shock sub can be used to mitigate a vibration generated by a vibratory tool or by bit rock interaction. In this regard, a model of the drill string is generated for real oil drilling at higher depth in commercial simulation software. This model includes self-weight, buoyancy forces due to the drilling fluid and realistic boundary conditions. This drill string model is used to predict the vibration tool force transmission to the rock and to the surface. This model is then used to design isolators to mitigate the vibration transferred to the surface. The result of this analysis shows that weight on bit (WOB), damping and spring constant of a shock sub have strong effects on the amplitude of vibration for the surface equipment. By applying higher WOB, damping and spring constant this amplitude would be reduced dramatically.

ACKNOWLEDGEMENTS

I would like to express my special thanks of gratitude to my graduate supervisors, Dr. Stephen Butt and Dr. Geoff Rideout who gave me the golden opportunity to work on a part of this advanced project for oil and gas drilling, which also helped me in doing this research and I came to know and discover new technologies and opportunities.

I would like to also thank Farid Arvani, the project manager for his support and encouragement.

I would like to also thank the Atlantic Canada Opportunity Agency (AIF Contract no.781-2636-1920044), Husky Energy, and Suncor Energy for funding this research over the past two and a half years. Additionally, the financial and academic support of the Faculty of Engineering and Applied Science is graciously acknowledged.

My special thanks to Moya Crocker and Dr. Leonard Lye for their help and supervision.

Last but not least, I would like to dedicate my thesis to my mother, Zaman and my best friend, Hamide for their endless support.

Table of Contents

DRILL STRING AXIAL VIBRATION AND SONIC HEAD ANALYSIS	i
ABSTRACT.....	ii
ACKNOWLEDGEMENTS	iv
Table of Contents.....	v
List of Tables	vii
List of Figures.....	viii
List of Symbols, Nomenclature or Abbreviations	xii
Symbols and Elements Related to Bond Graphs	xiii
Abbreviations.....	xiii
Chapter 1 : Introduction	1
1-1: Vibration assisted rotary drilling project (VARD group).....	1
1-2: Vibratory drilling with the Sonic Head Drilling (SHD).....	2
1-3: Drill string vibration	4
1-4: Objective of the research and thesis statement.....	5
Chapter 2 : Literature review on vibration and methods drill string isolation.....	8
2-1: Rotary percussive drilling.....	8
2-2: Types of vibratory assisted rotary drilling.....	10

2-3: The vibration behavior of the drill string.....	16
2-4: Shock sub analysis.....	26
2-5: Description of the next chapters	32
Chapter 3 : Sonic Head Drill simulation and vibration generation device for drilling analysis.....	34
3-1: Bond Graph	34
3-1-1: Power variables of bond graphs	38
3-1-2: Bond graph standard elements	38
3-2: Sonic Head Drill (SHD) bond graph modeling.....	50
3-2-1: Computing spring and damper coefficients	52
3-2-2: Experimental testing and damping and spring coefficients analysis	55
3-2-3: Dynamic model	62
3-3: Vibratory System Design	70
Chapter 4 : Axial Vibration in Drill String	76
4-1: Modal expansion, lumped model and finite element model (ABAQUS).....	77
4-2: Force analysis in the lumped model	90
4-3: Shock sub analysis and study	96
Chapter 5 : Concluding Remarks and future work	107
References.....	110

List of Tables

Table 3.1 The experimental test matrix	56
Table 3.2 The constants and parameters used in the dynamic model	65
Table 4.1 Drill pipe characteristics	80
Table 4.2 Natural frequencies for different models	85
Table 4.3 Drill collar characteristics	88
Table 4.4 Shock sub analysis parameters.....	101
Table 4.5 Sample test runs	102

List of Figures

Figure 2.1 Vibratory assisted drilling [76].....	11
Figure 2.2 NovaTek hydraulic hammer [9]	12
Figure 2.3 Resonance enhanced drilling, 1 is a polycrystalline diamond (PDC) drill bit, 2 is a vibro-transmission section, 3 is a piezoelectric transducer, 4 is a coupling and finally 5 is a drill string [69].....	13
Figure 2.4 Vibratory drilling system [11].....	14
Figure 2.5 Sonic drilling [12].....	15
Figure 2.6 Picture of a drill rig [29].....	18
Figure 2.7 Different types of stabilizer [30]	18
Figure 2.8 Axial, torsional and lateral vibration in the drill string [46].....	20
Figure 2.9 Imbalance in an assembly will cause centrifugally induced bowing of the drill string [2].....	21
Figure 2.10 A simple model for the axial vibration of the drill string [54]	23
Figure 2.11 Axial vibration of the drill string [56]	25
Figure 2.12 Schematic of the drill string with shock sub without damping [49].....	27
Figure 2.13 Kubanets shock absorber [62]	29
Figure 2.14 Torque Feedback Schematic [63]	30
Figure 2.15 Schematic of the AVD Tool [67]	31
Figure 2.16 Detailed View of the MRF Damper [67].....	32
Figure 3.1 Energy domains in Bond graph [71]	36

Figure 3.2 A model with physical parameters [71].....	37
Figure 3.3 Simplified bond graph with most of the bond graph elements [71].....	37
Figure 3.4 Bond graph resistance element [57].....	39
Figure 3.5 Bond graph compliance element [57].....	40
Figure 3.6 Bond graph inductance element [57].....	40
Figure 3.7 Bond graph energy source [57].....	41
Figure 3.8 Bond graph flow source [57].....	41
Figure 3.9 Bond graph transformer [70].....	42
Figure 3.10 Bond graph gyrator [70].....	44
Figure 3.11 Bond graph one junction [70].....	46
Figure 3.12 Bond graph zero junction [70].....	47
Figure 3.13 Half arrow: direction of power, E : element, J : junction [70].....	48
Figure 3.14 Prime mover with a smart speed governor [70].....	48
Figure 3.15 Causality between the prime mover and the load [70].....	49
Figure 3.16 Causal strokes for C, I and R elements [70].....	50
Figure 3.17 Causal stroke for effort and flow source [70].....	50
Figure 3.18 Rubber isolator mounted on the hydraulic actuator.....	52
Figure 3.19 a) Schematic; b) Work diagram of total force vs. displacement, showing slope equal to stiffness; c) Work diagram with damping force only [74].....	53
Figure 3.20 Effect of calibration and filtering on 20 Hz vibration at 1 mm amplitude.....	57
Figure 3.21 Spring constant, the slope of the dashed line.....	58
Figure 3.22 Work diagram.....	59

Figure 3.23 Damper force versus velocity	59
Figure 3.24 Change in the spring constant (kN/mm) with frequency (Hz) and amplitude (mm).....	60
Figure 3.25 Change in the damping coefficient (kN.s/mm) with frequency and amplitude (mm).....	61
Figure 3.26 System schematic	63
Figure 3.27 Bond Graph model of SHD	64
Figure 3.28 Force profile (kN) on the SHD frame, generated force and the force in the drill pipe for $f = 150$ Hz	66
Figure 3.29 Cover force amplitude divided by generated force amplitude	67
Figure 3.30 Ratio of transmitted force to the drill string and the generated force at each frequency.....	68
Figure 3.31 Generated force (kN) vs. frequency (Hz).....	69
Figure 3.32 Vibratory device for rotary drilling	71
Figure 3.33 Vibration generation device	72
Figure 3.34 Unbalanced mass attached on each gear and its properties.....	73
Figure 3.35 Generated force at 4 Hz.....	74
Figure 4.1 Lumped model.....	78
Figure 4.2 Modal expansion model of the drill pipe with 5 modes	81
Figure 4.3 ABAQUS model (first mode shape).....	84
Figure 4.4 Frequency vs. mode shapes for lumped and modal expansion models.....	86
Figure 4.5 Self-weight is added to a lump in a lumped model	87

Figure 4.6 Lumped model frequency accuracy for different combinations of lumps.....	89
Figure 4.7 Lumped model for the drill string with hook load at the top and fixed at the bottom	90
Figure 4.8 Archimedes' principle for objects submerged in fluids [78]	91
Figure 4.9 Effect of hydraulic pressure on axial forces in drill string: a) Schematic of drill string, b) Free body diagram for drill collars and c) Free body diagram for drill string section [78].....	92
Figure 4.10 Force vs. time for lumps 9 and 10 at 1800 and 2000 meters.....	93
Figure 4.11 Transition of tension to compression between the drill pipe and collar.....	94
Figure 4.12 Force versus axial position for the drill string.....	95
Figure 4.13 Force versus displacement for the drill string	96
Figure 4.14 Axial displacements vs. time for lumps 8 to 10	97
Figure 4.15 Axial displacements vs. time for lumps 28 to 30	98
Figure 4.16 Axial displacement vs. time for lumps 73 to 75.....	99
Figure 4.17 Axial displacement vs. time for lumps 73 to 75 with the SHD at 25 Hz	100
Figure 4.18 Rotary table displacement amplitude vs. WOB and damping coefficient.....	103
Figure 4.19 Rotary table displacement amplitude vs. WOB and spring coefficient.....	104
Figure 4.20 Damping and spring coefficient interaction	104
Figure 4.21 Rotary table displacement amplitude vs. WOB and location of the shoe sub	105
Figure 4.22 Rotary table displacement amplitude vs. damping and spring coefficient...	106

List of Symbols, Nomenclature or Abbreviations

a	Amplitude
b	Damping coefficient
bd	Damping coefficient for the drill pipe
br	Damping coefficient for the rock
E	Elastic or Young's modulus of rock
f	Frequency
F	Applied normal force
Ff	Friction force
Fr	Sonic Head Drill generated force
Fspring	Spring force
Fdamper	Damper force
G	Shear modulus
k	Spring stiffness
kr	Spring constant for the rock
kd	Spring constant for the drill pipe
m _{bit}	Bit and inner rod mass
m _u	Unbalanced mass
W _{sonic head}	Weight of the SHD
x	Bit displacement
ν	Poisson's ratio

ρ Density

Symbols and Elements Related to Bond Graphs

C Capacitive element

e Efforts source

f Flow source

I Inductive element

p Momentum

q Displacement

R Resistive elements

Se External effort source

V Velocity

Abbreviations

BHA Bottom-Hole-Assembly

BHP Bottomhole Mud Pressure

BOP Blow-out-preventer

DRI Drilling Research, Inc

DTH Down-the-hole hammer

FEM Finite Element Method

ROP Rate of Penetration

WOB Weight on bit

Chapter 1 : Introduction

Drilling is one of the major methods of exploration and exploitation of oil and gas reservoirs. Drilling techniques have been rapidly evolving to increase production rates while decreasing cost. Simple rotary drilling techniques have been replaced with advanced percussion or vibration drilling to achieve higher efficiencies. With the advancement of drilling methods, new areas of research will develop to enhance the drilling process. Some of these areas focus on the side effects of this advancement in drilling methods. Implementation of vibration in rotary drilling has led to analyzing the effect of the imposed vibration to drill rigs and in particular to the drill string. The drill string is one of the major parts of any drill rig and many important drilling parameters are controlled through the drill string to the bit. Control and isolation of unwanted vibration of this giant structure has a great effect on the drilling process and its efficiency.

1-1: Vibration assisted rotary drilling project (VARD group)

The vibration assisted rotary drilling (VARD) project is a 6 year research project which deals with the effect of adding vibration to conventional rotary drilling, to improve the drilling efficiency. The aim of the project is to build a prototype, based on numerical and experimental investigation of the aforementioned methods. The VARD research consists of five major tasks:

- 1- Experimental drilling facilities
- 2- Numerical drilling simulator
- 3- Drilling optimization
- 4- Drilling prototype design

5- Field tests

There are currently several graduate students and faculty investigators involved in the project, investigating different areas of the project to eventually build the prototype. This thesis investigates the axial vibration behavior of the drill string under vibration by the imposed pulsating force caused by the VARD tool. It also investigates the use of isolation methods, using different parameters and scenarios to dampen the unwanted vibrations in the drill string. The project is led by Memorial University with Dr. S. Butt as the principal investigator and industry partnerships including ACOA, RDC, Husky Energy and Suncor Energy.

1-2: Vibratory drilling with the Sonic Head Drilling (SHD)

Applying vibratory force on the drill bit during a conventional rotary drilling is proven to increase the rate of penetration. In this study, a review of several vibration generation mechanisms is presented.

Before focusing this study completely on the vibratory mechanisms, several other mechanisms that increase the ROP in the rotary drilling are presented in chapter 2. These mechanisms are: percussive drilling, mud pulsation drilling, vibratory drilling using unbalanced masses, resonance enhanced drilling and electromagnetic system.

Drilling is a cutting process that uses a drill bit to cut or enlarge a hole in solid materials. Effective drilling systems must be capable of permitting continuous and straight penetration in all materials, which may vary from very soft to extremely hard. They must be capable of providing a constant diameter, stable (or temporarily stabilized) path at full depth, from which the drilling debris has been wholly removed, staying consistent with the needs of the specific

2

construction process it serves. They will employ appropriate combinations of thrust, torque, rotary speed, percussive effort and flush parameters to economically reach target depth. Sonic drilling was developed in the late 1940s [4] and is becoming increasingly popular where strong environmental restraints are in force. It is a dual-cased system that uses high-frequency mechanical vibration to provide continuous core samples, or simply to advance casings for other purposes, such as deep wells or freeze holes. The string is vibrated at continuously adjustable frequencies between 50 Hz and 150 Hz, and is rotated slowly in harder formations to evenly distribute energy and bit wear. The frequency is adjusted to achieve the maximum penetration rate by coinciding with the natural resonance frequency of the drill string. Resonance provides extremely high energy to the bit, and in soil it also laterally displaces the particles, greatly improving penetration rate. Penetration is optimized by varying vibration frequency and thrust parameters.

The SHD is a technologically advanced, hydraulically activated unit that imparts high frequency sinusoidal wave vibrations into a drill string to effectuate a cutting action at the bit face. The resultant cutting action forces a circular continuous core of the formation up into the drill string. Due to the high forces developed by the SHD and the external flush nature of the drill string, excess formation material generated by the cutting face of the bit is forced into the borehole wall thus resulting in the generation of no cuttings during the drilling process other than the generated core sample. Through the development of various sizes and types of tooling, boreholes of different depths and dimensions can be drilled using the sonic drilling method in most types of subsurface formations. It is proven that the SHD is an effective tool in soil drilling, so it is the focus of this study to determine if this tool could also be used in oil and gas projects.

The SHD, as one of the means to create vibration induced drilling was studied by Advanced Drilling Group (ADG) for feasibility, ease of use and effectiveness for oil and gas projects. The SHD under study creates 100kN at the maximum frequency of 150 Hz where the generated force is damped partially by four dampers surrounding the head and transferred to the drill string. However, it was not clear how these dampers are affecting the output force, so two dampers were acquired from the SHD manufacturer and a series of tests were performed on them to find the damping and spring stiffness. The data gathered by these tests was then interpolated to predict both the damping and spring stiffness, at each frequency using Design Expert [5]. The mathematical models found for damping and spring constant were then used in 20Sim [6] to predict the output force of the SHD after the force is damped out and the result is presented in chapter 3 where it is discussed whether this system is feasible and compatible with the ADG line of research. Based on the unbalanced rotating mass concept used in the SHD, a new vibration generation device is also analyzed in chapter 3. The device used the unbalanced mass concept and it further improves the SHD and other designs in this area.

1-3: Drill string vibration

In the process of drilling engineering, the basic forms of drill string vibration are axial vibration, lateral vibration and torsional vibration. In chapter 2, different forms of the drill string vibration are explained in details.

Drill string can cause drill equipment failure, fatigue and can reduce the ROP.

In this study, axial vibration is main focus and it is presented in chapter 4. In this chapter an axial drill string model is developed and a force analysis is presented for this model to show that this

model could be a realistic representation of an actual drill string. After showing the presence of the axial vibration, a shock sub sensitivity analysis is presented to mitigate this vibration. In the shock sub sensitivity analysis, the effect of WOB, damping coefficient, spring coefficient and the location of the shock sub relative to the drill bit on the rotary table axial displacement is analyzed and the results are presented.

1-4: Objective of the research and thesis statement

The ADG has been actively researching new drilling technologies to improve the Rate of Penetration (ROP). It has been suggested that vibration can increase the ROP in hard formation and ADG has reviewed several vibratory drilling mechanisms. Patents and papers are reviewed in this study to find the most feasible and effective tool to create the vibratory assisted drilling tool. Chapter 2 describes some of these mechanisms.

One of the mechanisms this study found appealing for creating vibration during drilling is the SHD. As previously mentioned, the output force however is not the force transferred to the rock surface, since the generated force is damped by four dampers surrounding the SHD's core and the damping effect of the drill string. One of the purposes of this study was to determine the effect of these dampers on the output force at each frequency and how much generated force is transferred to the SHD's frame. The ADG was in negotiation to purchase this device for laboratory and field test and it was necessary to estimate the output force on the drill bit and the force on the drilling frame. Two isolators were acquired and a series of tests were run to investigate the change in damping and spring stiffness at each frequency. The results are presented in chapter 3 along with the simulation software analysis.

After analyzing the benefits and shortcomings of the SHD, another vibration generation device based on the unbalanced mass concept used in the SHD, is studied and preliminary design and simulation results are presented in chapter 3. It is investigated how a vibratory force can be generated using the confined space available in the borehole and how this force can be controlled.

Another purpose of this study is to focus on the phenomena of drill string vibration; to gain insight into the role of the drill string and apply several methods to mitigate it.

A drill string model is established in a commercial simulation software (20Sim [6]), and its validity and effectiveness in having similar characteristics to an actual drill string is studied. In order to get a better insight into the drill string modeling, two design techniques (modal expansion and lumped segment model) and finite element software (ABAQUS) are used. The natural frequencies for all three models are compared to insure that all models behave the same under vibration. The SHD model developed in this study is then implemented in the model to investigate how vibration would travel through the drill string to a bit and to the earth surface. Different forces and conditions are applied to this model to cover a wide range of scenarios in this study.

Axial vibration can reduce the ROP and cause severe damage to wellbore and surface equipment. In the last section of chapter 4, implementations of dampers or shock subs on reducing the axial vibration are investigated. Damping coefficient, stiffness coefficient, WOB and shock sub location are varied to find a mathematical model predicting surface displacement and force transferred to the bit.

To recap, the motivation of this study is to investigate the feasibility of the SHD for the ADG and to develop a modified design based on the concept used in the SHD. It is also the motivation of this study to develop an axial drill string model and study the effect of the SHD on this model and introduce methods of mitigating this vibration.

Chapter 2 : Literature review on vibration and methods drill string isolation

2-1: Rotary percussive drilling

Development of a more efficient and cost-effective drilling technology will significantly increase oil and gas production by allowing economic exploitation of difficult formations (such as deep, hard rock reservoirs). Potential savings of \$200 to \$600 million are possible if the penetration rate in the hard rock can be doubled while maintaining the bit life [79].

There is evidence that the combination of percussion and rotary drilling techniques can potentially provide significant improvement in the rate of penetration in hard rock environments. In addition to faster penetration, other benefits include the ability to use lower weight on the bit, less contact time with rock and therefore less abrasion, longer bit life and improved hole deviation control [14].

Colonel F. L. Drake was the first person to use a cable tool percussion type machine for oil well production in 1859. The first technical report of percussion drilling technique was submitted in 1949 by Harpst and Davis [80]. This report resulted in the creation of several different terms, all of which are used to describe this type of drilling. Examples include percussion hammer, down hole hammer, percussive drill, percussive rotary drilling, etc.

Between 1950 and 1960, there were substantial laboratory research breakthroughs on this subject [81]. Percussive drilling was not a commonly accepted method until the 1980's, due to frequent mechanical failures, poor analytical understanding of the method, and economical uncertainties and inability to control the drilling parameters [82]. In 1981, Pratt [82] reported the results of the

application of percussion drilling with an average time for TVD (total vertical depth) of 80 days. This was a definite improvement over the conventional mud drilling methods, which took 103 days to drill the same well. Also a cost per foot reduction of 49% was achieved with hammer bits [14]. In another survey it was reported that percussive rotary drilling could be 7.3 times faster than the conventional rotary method [83]. Fluid hammers appeared first in 1990 [14]. After the first appearance of the fluid hammer in 1990, energies were focused on improving hammer design and performance. These hydraulic or water hammers have been used to conduct drilling in hard rock formations since their appearance in 1990, as air hammers are limited by penetration depth [84].

In rotary percussive drilling, the rock is broken by repeated impacts and the rotation imposes a new point of impact every time. The rock is thereby broken, crushed and flushed out from the hole. The advantage with rotary percussion drilling is that rock fails due to dynamic loading rather than crushing the rock through static loading as in conventional rotary drilling [82]. More than 2000 cyclic loadings per minute can be applied to the bit, which generate high stress in a short time. This causes the penetration in hard formations to be more effective than rotary drilling with its lower stresses and long time of static load application. Therefore, percussion drilling transmits power to the bit more efficiently than rotary drilling.

With higher and more consistent penetration rates than rotary methods (by a factor of 5 or more), percussion drilling provides relatively small, light, and mobile drill rigs and low drilling costs [85].

The hammers can be categorized into top hammers and down-the-hole-hammers. Gas and air, hydraulic, fluid and jet assisted rotary percussion hammers are common means of providing percussion force to the bit [9].

The main difference between the percussive and vibratory drilling is that in percussive drilling, short rapid thrust or force is applied on the rock being drilled, whereas in the vibratory drilling the force follows a sinusoidal path to be applied on the rock being drilled. In the next section several vibration assisted rotary drilling devices are reviewed.

2-2: Types of vibratory assisted rotary drilling

Several vibratory assisted drilling mechanisms are proposed to increase the ROP. The vibratory unit for drilling [76] shown below uses hydraulic power to rotate the unbalanced gears. The horizontal forces cancel each other out when the unbalanced masses are at 0 and 180 degrees, and they add to the WOB and apply a vibratory force when they are at 90 and 270 degrees.

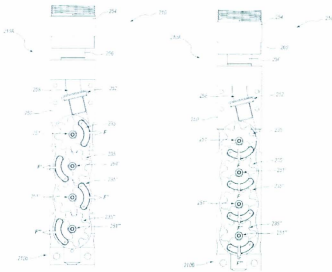


Figure 2.1 Vibratory assisted drilling [76]

In other studies by two companies, Orion and Tempress [77], drilling fluid fluctuation is used to create vibration near the bit. In these studies, an increase in the ROP up to 55% was recorded by field studies. In both systems, an electromagnetic valve mechanism opens and closes for a short time interval, changing the drilling fluid pressure.

In another study by NovaTek [9], a percussive drilling hammer was designed to increase the ROP by up to 33% in a laboratory testing (Figure 2.2). However in some of the tests done at the Terratek [10] facilities, ROP showed negligible change due to bottom hole pressure. It is the intent of this research to investigate the design of vibratory systems and provide models that could be used in similar test to further study the effect of vibration on drilling.

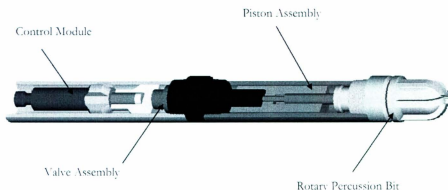


Figure 2.2 NovaTek hydraulic hammer [9]

In another study, a drill bit capable of rotary and high frequency oscillatory loading (Figure 2.16) is designed where the system has a means of controlling applied rotational and/or oscillatory loading for the drill bit [69]. The control system of this apparatus measures the responsive condition of the material through which the drill string is passing and measures the natural frequency of the rock using sensors and under closed loop real time measurement, adjust the frequency of oscillation to increase the ROP (Figure 2.3).

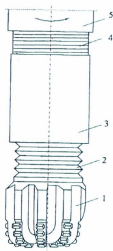


Figure 2.3 Resonance enhanced drilling, 1 is a polycrystalline diamond (PDC) drill bit, 2 is a vibration transmission section, 3 is a piezoelectric transducer, 4 is a coupling and finally 5 is a drill string [69]

Bodine A. G. [11] has designed a vibratory device that uses unbalanced masses and drilling fluid hydraulics to increase the ROP (Figure 2.4). In this apparatus, a turbine-operated vibratory device is propelled by the drilling fluid. The rotating shaft of the turbine is geared to turn a series of weighted rotors mounted on horizontal shafts below the turbine. The rotors are weighted on one side so that when they revolve, force is exerted on the shafts. Adjacent rotors turn in opposite directions and the rotors are set so the forces produced are additive in the vertical direction and cancel in the horizontal direction. Drilling rates as high as 30 feet per hour in granite have been obtained, using 120 feet of drill collars, a circulation rate of 300 to 400 USGPM and a frequency of 60 Hz [11].

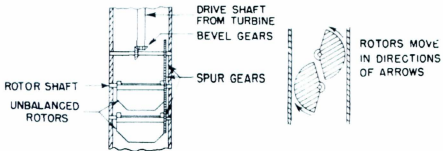


Figure 2.4 Vibratory drilling system [11]

A casing is brought into a vibration within the hearing range (150 Hz). These waves are sent to the casings' lower end and reflected, causing the casing to stretch and get thinner or to shorten and get thicker some 150 times per second. This intense "massage" causes a very thin layer of soil particles, directly surrounding the casing, to enhance the movement of the structure. Instead of a stiff mass the soil starts behaving like a "fluid" powder (unsaturated zone dry bedrock) or as slurry or paste (saturated zone bedrock). This fluidization or better said, liquefaction severely reduces friction between casing (or soil sampler) and soil. In practically all soil types this reduction allows very rapid penetration speeds in combination with a low rig weight. When taking soil samples, the same friction reduction counts for the inner wall of the sampling device. It is also proposed that varying the WOB can increase the ROP. Figure 2.5 shows how the SHD works:

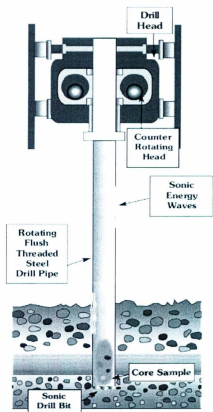


Figure 2.5 Sonic drilling [12]

As shown in Figure 2.5, the SHD's core is surrounded by four dampers that are connected to the frame and make sure that the generated force is transferred to the drill pipe.

Design of the SHD has gone through many changes since the 1940s [12].

The ADG has been actively investigating drilling techniques, specifically vibration generation devices for drilling. One of the main purposes of the ADG project is designing and manufacturing a drilling rig that can create vibration during rotary drilling. The SHD is

prominently used in soil drilling and this thesis to investigate affordability and ease of use of this tool for oil and gas drilling. The control over output force and the effect of the dampers surrounding the SHD on the output force are studied in chapter 3.

2-3: The vibration behavior of the drill string

Drill string vibration has been a challenging issue for drillers in oil fields for a long time. The effects of vibration on the drilling performance, wellbore stability, joint failures, fatigue etc, has convinced drilling companies to strengthen components, or try to control and mitigate these effects to attain higher performance [13][14]. In order to control or mitigate the vibration, its behavior and characteristics should be revealed and modeled analytically [15] [16] [17] [18] [19] [20] and experimentally in laboratory scale [21] [22] [23] [24], or through field verification [25]. The drill string is connected to a drill rig kelly at the rig and transfers rotary motion to the bit. WOB is applied on the bit through the buoyant weight of the drill collar [78]. Figure 2.6 shows the drill rig and the drill pipe next to it [29].

The drill string is under both tension and compression. Due to the hoisting load, mud hydrostatic effect and weight, drill pipes are mostly under tension and drill collars are under compression. The neutral point is defined as the place in the drill string where the tension stress changes to compression. The mud, which is being circulated to the bottom hole, serves the dual purpose of cooling the bit as well as flushing the cuttings. WOB usually changes between $10^4 - 10^5$ N and torque which is provided as the top rotates the drill string with the speed of 50-200 rpm [26].

The stabilizers are provided at the drill collars section to prevent vibration and buckling of the drill string and to stop the unwanted deviation of the drilling trajectory. The distance between stabilizers along the collar section varies between 5 to 50 m. A schematic of stabilizers are shown in Figure 2.7.

The drill collars, bit and stabilizers are usually called the bottom hole assembly or BHA. The majority of drill string failures occur at this section. Due to the higher stiffness and higher mass of the BHA with regard to the pipe section, the vibration behavior of the drill string is mostly influenced by the BHA vibration behavior [27]. This dominant role of the BHA vibrations on the total drill string vibration was verified by Dareing [27], who showed that the collars are easily excited in the lower modes. The pipes act as if they are rigid and do not vibrate during such excitation [28].



Figure 2.6 Picture of a drill rig [29]

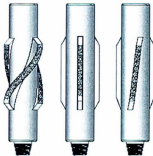


Figure 2.7 Different types of stabilizer [30]

Unwanted vibrations of the drill string dissipates some part of the provided energy, which is supposed to be delivered to the bit. The unwanted vibration may result in hole deviation, lower

penetration rate, premature failure and lower efficiency of the drilling process. Therefore, a thorough understanding and an ability to isolate the unwanted vibration is essential to the design of the drill string. Vibration however could not be damped by 100%.

The primary modes of drill string vibrations are axial, lateral and torsional [31] [32] [33] as shown in Figure 2.8.

Axial vibration (Figure 2.8) can cause bit bounce, which may damage bit cutters and bearings.

Axial vibration is most common in vertical holes when drilling hard formations. It can be detected at the surface. Accelerated bearing and tool wear, seal failure, broken tooth cutters, failure of the measurement while drilling (MDW) tools and reduction in ROP are most common results of axial vibration and bit bounce [47].

Torsional vibrations can cause irregular down-hole rotation. Stick/slip is often seen while drilling and is a severe form of drill string torsional oscillation in which the bit stops rotating for a period. As the severity of stick/slip increases, the length of the stuck period increases, along with rotational acceleration as the bit breaks free.

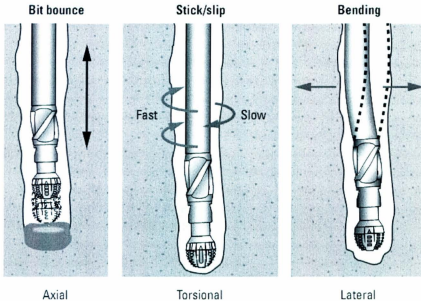


Figure 2.8 Axial, torsional and lateral vibration in the drill string [46]

Torsional vibration (Figure 2.8) fatigue the drill collar connection and can damage bits. The use of a mud motor may help to address stick/slip if the main source of excitation is from the bit, but the presence of a motor does not prevent stick/slip. The drill string and bottom hole assembly (BHA) above the motor, can enter into a stick/slip motion even when the motor is turning the bit at a steady rate [46].

Lateral vibrations (Figure 2.8) are the most destructive type of vibration and can create large shocks as the BHA impacts the wellbore wall. The interaction between BHA and drill string contact points may, in certain circumstances, drive the system into backward whirl. Backward whirl is the most severe form of vibration, creating high-frequency large-magnitude bending moment fluctuations that result in high rates of component and connection fatigue. Imbalance in

an assembly will cause centrifugally induced bowing of the drill string, which may produce forward whirl and result in one-sided wear of components (Figure 2.9).

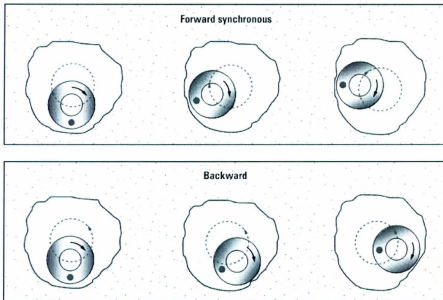


Figure 2.9 Imbalance in an assembly will cause centrifugally induced bowing of the drill string [2]

Vibrations of all three types (axial, torsional, and lateral) may occur during rotary drilling and are coupled. Induced axial vibrations at the bit can lead to lateral vibrations in the BHA. Axial and torsional vibrations observed at the rig floor may actually be related to severe lateral vibrations downhole, near the bit. At other times, severe axial vibrations near the bit may show no visible vibrations at the surface.

Axial and lateral vibrations are more violent in vertical or low-angle wells, and the displacement and bending moments introduced by lateral vibrations increase as the ratio of hole size or BHA collar size increases [46].

A drill string vibrates as a result of load or displacement excitations applied at various locations and frequencies. There is a wide range of potential excitation sources: imbalanced masses, misalignment, kicks or bends, the cutting action of the drill bit, stabilizer blades (especially if they are straight), mud motors (nutating, wobbling of the rotor within the stator), and the friction factor between the drill string and borehole wall.

In most cases, pulling off bottom, changing the rotational speed or weight on bit (WOB) can reduce the axial vibration [48]. In the drilling situations where axial vibration is happening most of the time, installing a shock sub can reduce the vibration in the bottom hole through changing the resonance frequency of the drill string. This application will be explained in detail in chapter 4 detailing isolation methods. Since the drill string makes the hole parallel to its axis, axial vibration plays an important role in the trajectory deviation and ROP [49].

A variety of models have been used to investigate these vibrations. Continuous models were used in early studies to model drill strings [50] [51] [52] [53], while more recently, finite element models have been applied to axial vibration investigations [54]. Some studies, however, have not used a complete model for drill strings, but have focused only on BHA's e.g. [55]. This is due to the fact that BHA is placed right above the bit and it has more contact with the well bore. Figure 2.10 shows one of the models used in the previous research to study axial vibrations of drill strings.

Implementation of damping into models is an important aspect of the studies of axial vibrations. Some investigations did not consider any type of damping, e.g. [50]. While others researchers incorporated damping mechanisms into their models [51] [52] [53] [54]. The two most common types of damping used include: simple viscous damping [51] [53] and frequency-dependent damping [54] which after the analysis done in Chapter 3 shows the latter is more important.



Figure 2.10 A simple model for the axial vibration of the drill string [54]

Over the years, a great deal of research has been completed to investigate the effects of different parts of the drill string on its axial vibrations. For example, Kreisle [53] showed the importance of a shock sub in reducing axial vibrations and Dareing [27] revealed the dominant effect of drill collar length on axial and torsional vibrations of drill strings.

In order to reach a better prediction of drill string axial vibrations, it is important to model the excitations accurately. This subject, therefore, has been one of the main areas of investigation of drill string vibrations. Daring [55] identified various sources of excitation, such as pump pressure, sidewall friction, and drill bit/formation interaction. He also indicated that the various types of drill bits (i.e., roller cone, diamond, PDC) generate different loading conditions to the bottom end of the drill string. A harmonic excitation is the main mechanism used in previous studies of drilling with roller cone bits. This harmonic excitation has been expressed in terms of sinusoidal motion, which is applied at the bit [52]. Due to the rolling of the bit, a multi-lobed surface is formed on the formation; the number of lobes formed depends on the number of cones on the bit. This lobed-pattern can be defined by a profile with sinusoidal angular variation elevation [54].

The classical equation for axial vibration of a bar (Figure 2.12) is as follows:

$$E \frac{\partial^2 u}{\partial x^2} - \xi \frac{\partial u}{\partial t} - \rho \frac{\partial^2 u}{\partial t^2} - \rho g = F_c(x, t, u) \quad (2.1)$$

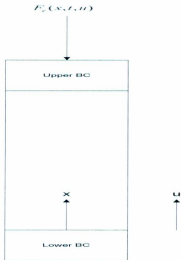


Figure 2.11 Axial vibration of the drill string [56]

ρ is the density per unit volume, ξ is the damping factor and E is the Young's Modulus, and $u(x, t)$ is the longitudinal displacement of the bar element.

$E \frac{\partial^2 u}{\partial x^2}$ is the result of difference between normal stress $E \frac{\partial u}{\partial x}$ acting on the face of control mass and $E \frac{\partial u}{\partial x} + \partial(E \frac{\partial u}{\partial x})$ acting on the opposite side. $\xi \frac{\partial u}{\partial t}$ refers to viscous dissipation and ρg refers to the static weight. $F_e(x, t, u)$ represents the excitation forces, external forces and displacement sources in the axial direction. According to the free-fall limit theory, $\frac{\partial u}{\partial t} < 0$ means advance motion toward the hole or making hole and $\frac{\partial u}{\partial t} > 0$ means bit bounce [57].

A lot of uncertainties exist regarding the modeling of the boundary condition of the drill string in the axial mode. Some have assumed the top boundary condition as being fixed and neglected the

25

mass and stiffness of the swivel and traveling block, as well as the stiffness of elastic wire cable and the derrick [39]. One suggestion is that the derrick and the draw wires should be modeled as a mass-spring-damper system. Clayer [58] verified that this model is sufficiently accurate for surface modeling. At the lower end, the cutting action of the rock gives rise to the bit motion, which is a periodic motion. Therefore, at the bit, a harmonic displacement boundary condition could be assumed. The displacement could be assumed as $u(L,t) = u_0 \sin(\omega t)$, where for the tricone bits, ω is three times the bit rotary speed and u_0 is the peak to peak cone vertical displacement [52]. Fixed displacement boundary condition at the lower end could be assumed for hard rock drilling. In summary, three sets of boundary conditions were assumed in the literature for axial vibration of the drill string [39] [58] [52] [49]:

- 1- Fixed-fixed B.C (boundary condition)
- 2- Fixed at top-free at the bottom
- 3- Equivalent mass-spring-damper at the top and displacement at the bottom

It is obvious that the last case is the most realistic case and hence it is used for drill string analysis in this study. The displacement at the last set for the lower boundary condition could be assumed as a way of establishing the other sets of the boundary conditions.

2-4: Shock sub analysis

To control the axial vibration of the drill string, shock subs are mainly used. The shock subs are composed of a spring damper system which is installed between the bit and the drill collars. A simple model of shock sub can be found in the work by Kreisle [49] (Figure 2.13). In this model,

the lower boundary condition for the boundary value at the shock sub point is set as a spring force, which should be equal to the force at the bottom of the drill collars. For the spring force, the author assumed a harmonic displacement at the bit. He solved the boundary value problem of the axial vibration, using the Laplace method. According to his results, it can be understood that the shock sub will dampen the drill string vibration through a phase shift between the force and displacement at the bit. This is on the contrary to the common belief that the change in the resonance frequency due to shock sub installation is the main cause of damping [49].

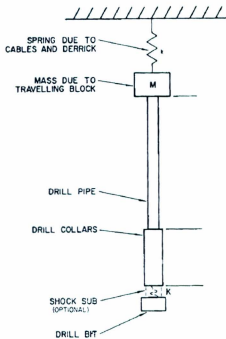


Figure 2.12 Schematic of the drill string with shock sub without damping [49]

Elsayed [59] proposed a method to analyze design parameters of shock subs. Springs that are too weak or too stiff do not lead to vibration reduction. They modeled the shock sub as a damped spring mass system and used Matlab Simulink[®] [60] to analyze the problem. They computed RMS values for different combinations of the shock absorber parameters and found an optimum value for these parameters. Their analysis was in the time domain. The results were presented for different damping ratios as well as different natural frequencies of the shock sub. They suggested Magneto-Rheological dampers to achieve the desired damping ratio.

Several types of dampers were studied to have a better understanding of damper specification and the way they work.

Chen [61] presented the results of shock sub performance testing for three different shock subs from six manufacturers. From the results it was noted that a mechanical shock sub, from an undisclosed manufacturer, provided the best damping of axial accelerations. The shock sub contained a Belleville spring, using friction between the springs as the primary damping mechanism. Fluid damping can augment this. During testing, this damper reduced axial vibrations approximately 23% and lateral vibrations approximately 51% (at the top). It can also be noted that the bit sensor recorded axial and lateral vibrations almost identical both with and without the presence of a damper.

Other mechanical dampers include the three shock absorber designs presented in [62]. The first design presented is named Kubanets, and was designed in 1964, see Figure 2.13.

Later designs of the Kubanets shock absorber absorb axial vibrations by using rubber rings of circular cross section, placed in a special metal casing and assembled as a separate upper section.

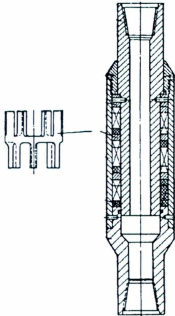


Figure 2.13 Kubanets shock absorber [62]

An active damper responds to feedback, whether it is electrical signals or mechanical responses, and adjusts one or more parameters to control vibrations and the amount of damping provided. Halsey [63], states that using a torque feedback control system can produce a more uniform motion of a drill string. Such a control system can stop stick-slip motion and prevent it from starting. Additionally, such a control system leads to smoother rotation of the bit which in turn, can lead to a reduction in axial and lateral vibrations of the drill string. Allowing the rotary table or top drive speed to respond to dynamic torque oscillations in such a way, that the rotary system absorbs or dampens the vibrations, is the main concept behind torque feedback [63]. Figure 2.15 illustrates an example of a torque feedback loop [64].

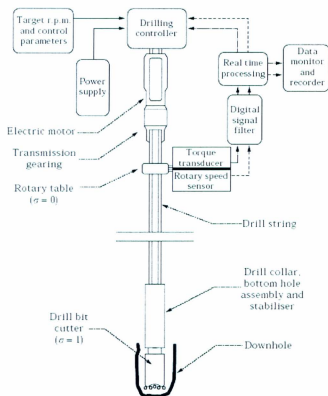


Figure 2.14 Torque Feedback Schematic [63]

As a more general description of active damping utilizing feedback, U.S Patent No. 5,117,926 [66] describes controlling vibrations in borehole equipment by defining energy flow through the equipment as the product of an across variable and a through variable. The patent states that by measuring fluctuations in one variable, the other can be adjusted such that the energy flow remains within desired limits. These limits are chosen such that the minimum reflection of energy waves from down-hole occurs at the rotary table. For a rotary drive, energy flow can be defined as torque times angular velocity [65].

Barbely [67] discussed the results of drilling tests of an active vibration damper. The Active Drilling Vibration Damper (AVD) studied was structurally similar to a shock sub, with the absorber filled with magnetorheological fluid (MRF) rather than the traditional hydraulic oil. MRF is a suspension of fine iron particles in a fluid (generally oil), which instantaneously increases its viscosity under the influence of a magnetic field. By using a series of coils to induce intense electromagnetic fields, the damping coefficient of the fluid can be increased by a factor of 7-10 in milliseconds. The AVD “has a torsional bearing and a Belleville spring stack. The upper portion contains the APS [Advanced Products and Systems] high temperature (200 C°) turbine-alternator to supply power.” Feedback from a linear motion detector, in response to drill bit motion, controls the AVD. The AVD and MRF damper can be seen in Figures 2.16 and 2.17.



Figure 2.15 Schematic of the AVD Tool [67]

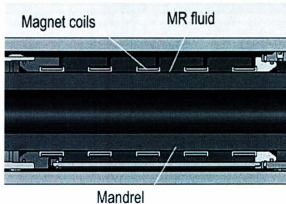


Figure 2.16 Detailed View of the MRF Damper [67]

Controlled drill string vibration is used to enhance drilling performance [68]. This improvement can be achieved either through mitigating the vibration in the BHA or using the effect of resonance to increase the vibration force and hence increase the ROP. Bakenov (2003) used resonance vibration calculations to improve ROP by adjusting the drill string revolutions, and potentially reflect dynamic load waves back to their source, i.e. the bit, through implementation of an additional drill string component such as a shock absorber or incorporating different drill string materials. The positive effects of losing contact across the chamfers is also reviewed in his study in order to utilize all energy for the cutting process and after thorough analysis a parametric maps have been developed to demonstrate quantitative relationships.

2-5: Description of the next chapters

In the following chapters, vibratory tool design, the SHD analysis and axial vibration in drill string are presented. In chapter 3, the SHD design and operation is demonstrated and a series of

tests done on dampers surrounding the SHD's core are detailed. Analysis and simulation results are presented for the SHD output force and the force on the bit and the effect of isolators is explained. Later in chapter 3, a new CAD designs for vibration generation devices are demonstrated and simulation results for one of these devices is presented.

Drill string axial vibration is the main focus of chapter 4, where different boundary conditions and vibratory forces are applied to a drill string and the effects of these changes are analyzed.

Later on, the effect of isolation on mitigating vibrations in a drill string is analyzed and the effect of WOB, damping coefficient, spring coefficient and the location of an isolator on the amplitude of vibration at the surface is discussed.

Chapter 3 : Sonic Head Drill simulation and vibration generation device for drilling analysis

This chapter gives an overview on the SHD (Sonic Head Drill) design and analysis, and a design of a vibration generation device for rotary drilling.

In the first section, a brief overview of bond graph methodology is presented, as it is used in SHD modeling and axial vibration analysis in chapter 4. In section 3-2, an in-depth analysis on SHD is detailed. The SHD is used to increase the ROP in soil drilling. The core of a SHD is surrounded by four isolator and it is the purpose of this chapter to study the change in isolators' damping and spring coefficients with frequency, and apply them in a model to predict the force transferred to a drill string and drill frame. The last section of this chapter gives a brief summary of a vibratory device design that uses unbalanced masses concept used in SHD to create vibration for rotary drilling.

3-1: Bond Graph

Bond graph methodology was introduced by Henry M. Paynter, professor at MIT and UT Austin [70]. The term "Bond Graph" comes from the fact that many of these graphs look like the bonds in chemistry. Bond graphs are a graphical modeling language (examples of other graphical modeling languages are block diagrams and signal-flow diagrams) in which mechanical, electrical, thermo-fluid, and magnetic systems are represented with a small set of generalized energy storage, dissipation and transfer elements. Elements are connected with power bonds, each of which contains a pair of signals generally known as "effort" and "flow" whose product

gives instantaneous power of the bond. For an electrical system, effort and flow are voltage and current respectively, and for a mechanical system they are force and velocity. Half arrows on the bonds define the direction of positive power flow, and control signals are represented by lines with full arrows. Casual strokes, placed normal to one end of each bond, define whether or not an element has a causal flow or effort output when assembling system equations. Generalized Kirchhoff loops and nodes are represented by 0- and 1-junctions. Elements bonded to a 0-junction have common effort, and their flows algebraically sum to zero. Elements bonded to a 1-junction have common flow but the algebraic sum of their efforts is zero. Bond graphs facilitate the generation of governing equations, allow prediction of numerical issues such as implicit and differential-algebraic equations, and allow easy combination of electrical, mechanical and thermo-fluid sub-models. For more details about bond graph modeling see Karnopp [57].

The term presented above, are explained in more details in this section.

Energy domains with corresponding flow, effort, generalized displacement and momentum are shown in Figure 3.1:

	f flow	E effort	$q = \int f dt$ generalized displacement	$p = \int e dt$ generalized momentum
<i>Electromagnetic</i>	i current	U voltage	$q = \int i dt$ charge	$\lambda = \int u dt$ magnetic flux linkage
<i>mechanical translation</i>	V velocity	F force	$x = \int v dt$ displacement	$p = \int F dt$ momentum
<i>mechanical rotation</i>	ω angular velocity	T torque	$\theta = \int \omega dt$ angular displacement	$b = \int T dt$ angular momentum
<i>hydraulic/ pneumatic</i>	φ volume flow	P pressure	$V = \int \varphi dt$ volume	$l = \int p dt$ momentum of a flow tube

Figure 3.1 Energy domains in Bond graph [71]

Figure 3.3 shows a simplified bond graph with most of the bond graph elements which is created from the physical model in Figure 3.2. This diagram is composed of 1-junctions, 0-junctions, external effort source (Se) for force input, external flow source (Sf) for velocity input, capacitive element (C), resistive elements (R), generalized inductive element (I), transformer (TF) (TF adds no power but simply transform effort to effort and flow to flow) and gyrator (GY) (GY related flow to effort without adding any power). Typically, state variables in the bond graph formalism are generalized momentum (p) and displacement (q).

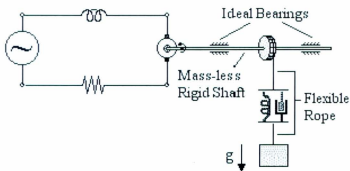


Figure 3.2 A model with physical parameters [71]

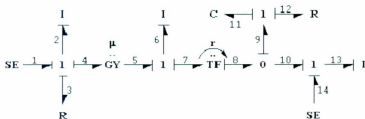


Figure 3.3 Simplified bond graph with most of the bond graph elements [71]

Bond Graph theory has been further developed by many researchers like Karnopp, Rosenberg, Thoma, Breedveld, etc. who have worked on extending this modeling technique to power hydraulics, mechatronics, general thermodynamic systems and recently to electronics and non-energetic systems like economics and queuing theory.

From the pictorial representation of the bond graph, the derivation of system equations is so systematic that an algorithm can be created. The whole procedure of modeling and simulation of

the system may be performed by some of the existing software e.g., 20Sim, ENPORT, Camp-G, SYMBOLS, COSMO, LorSim etc[57].

3-1-1: Power variables of bond graphs

The language of bond graphs expresses general physical systems through power interactions. The factors of power, for example effort and flow, have different interpretations in different physical domains which are shown in Figure 3.1. They could be used in several energy domains i.e. electrical, hydraulic, and thermal etc. [70]

3-1-2: Bond graph standard elements

In bond graph, one needs to recognize only four groups of basic symbols, i.e., three basic one port passive elements, two basic active elements, two basic port elements and two basic junctions. The basic variables are effort (e), flow (f), time integral of effort (P) and the time integral of flow (Q).

Basic 1-Port elements:

A 1-port element is addressed through a single power port, and at the port a single pair of effort and flow variables exists. Ports are classified as passive ports and active ports.

The passive ports are idealized elements because they contain no sources of power. The inertia or inductor, compliance or capacitor, and resistor or dashpot, are classified as passive elements.

R-Elements:

The 1-port resistor [57][70] [71] is an element in which the effort and flow variables at the single port are related by a static function. Usually, resistors dissipate energy. This must be true for simple electrical resistors, mechanical dampers or dashpots, porous plugs in fluid lines, and other analogous passive elements. The bond graph symbol for the resistive element is shown below.

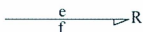


Figure 3.4 Bond graph resistance element [57]

The half arrow pointing towards R means that the power i.e., product of F and V (in a mechanical system) (or $e \cdot f$ in general terms) is positive and flowing into R , where e , represents effort or force, and f , represents flow or velocity. The constitutive relationship between e , f and R is given by:

$$e = R \cdot f \quad (3.1)$$

$$\text{Power} = e \cdot f = R \cdot f^2 \quad (3.2)$$

C-Elements:

Consider a 1-port [57] device in which a static constitutive relation exists between an effort and a displacement. Such a device stores and gives up energy without loss. In bond graph terminology, an element that relates effort to the generalized displacement (or time integral of flow) is called a one port capacitor. In physical terms, a capacitor is an idealization of devices like springs, torsion bars, electrical capacitors, gravity tanks, and accumulators etc. The bond graphic symbols, defining the constitutive relation for a C-element are shown below:



Figure 3.5 Bond graph compliance element [57]

In a spring, the deformation (Q) and the effort (e) at any moment is given by,

$$Q = \int f dt , \quad e = K \int f dt \quad (3.3)$$

Here, flow is the cause and deformation, and hence effort is the consequence. In a capacitor, the charge accumulated on the plates (Q) or voltage (e) is given by,

$$Q = \int i dt , \quad e = \frac{1}{c} \int i dt . \quad (3.4)$$

Here, the current is the cause and the total charge, and hence voltage is the consequence.

l-Elements:

A second energy storing 1-port [57][70] [71] arises if the momentum, φ , is related by a static constitutive law to the flow, f . Such an element is called an inertial element in bond graph terminology. The inertial element is used to model inductance effects in electrical systems and mass or inertia effects in mechanical or fluid systems. The bond graph symbol for an inertial element is depicted in Figure 3.6.



Figure 3.6 Bond graph inductance element [57]

If the mechanics of mass point is examined by considering the impulse-momentum equation, then we have;

$$\varphi = \int f dt \quad , \quad f = \frac{1}{m} \int e dt \quad (3.5)$$

Here, effort is the cause and velocity, and hence momentum is the consequence. Similarly the current in an inductor is given by;

$$i = \frac{1}{L} \int e dt \quad (3.6)$$

Effort and Flow Sources:

Active ports are those which give reaction to the source. For example, if one steps on a rigid body, one's feet react with a force or source [57]. For this reason, sources are called active ports. Force is considered as an effort source and prescribed motion of a rigid body requires a velocity source. They are represented as a half arrow pointing away from the source symbol. The effort source is represented by the following:



Figure 3.7 Bond graph energy source [57]

While the flow source is represented as shown below:



Figure 3.8 Bond graph flow source [57]

Basic 2-Port elements:

There are only two kinds of port elements, namely "Transformer" and "Gyrator". The bond graph symbols for these elements are TF and GY, respectively. As the name suggests, two bonds are attached to these elements.

The Transformer:

The bond graphic transformer [71] can represent an ideal electrical transformer, a massless lever, etc. The transformer does not create, store or destroy energy. It conserves power and transmits the factors of power with proper scaling as defined by the transformer modulus (discussed afterwards).

The meaning of a transformer may be better understood if one considers an example given below. In this example, a massless ideal lever is considered. Standard and bond graphic nomenclature of a lever are shown in Figure 3.9. It is also assumed that the lever is rigid, which means a linear relationship can be established between power variables at both the ends of the lever.

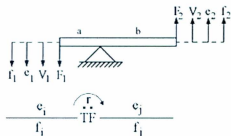


Figure 3.9 Bond graph transformer [70]

From the geometry we have the following,

$$V_2 = (b/a) V_1 \quad (3.7)$$

The power transmission implies

$$F_2 = (a/b) F_1 \quad , \quad \text{so that} \quad V_2 \cdot F_2 = V_1 \cdot F_1 \quad (3.8)$$

In bond graphs, such a situation may be represented as shown in the above Figure 3.9.

The 'r' above the transformer denotes the modulus of the transformer, which may be a constant or any expression (like 'b/a'). The small arrow represents the sense in which this modulus is to be used.

$$f_j = r f_i \quad , \quad \text{and} \quad e_j = (1/r) e_i \quad (3.9)$$

Thus the following expression establishes the conservation of power,

$$e_j f_j = e_i f_i \quad . \quad (3.10)$$

The Gyration:

A transformer [70] relates flow-to-flow and effort-to-effort. Conversely, a gyrator establishes the relationship between flow to effort and effort to flow, again keeping the power on the ports the same. The simplest gyrator is a mechanical gyroscope, shown in Figure 3.10.

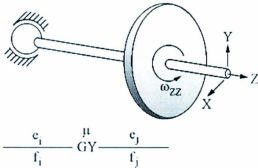


Figure 3.10 Bond graph gyration [70]

A vertical force creates additional motion in horizontal direction, and to maintain a vertical motion, a horizontal force is needed. So the force is transformed into flow and flow is transformed into force with some constant of proportionality. In this example, I_{zz} stands for moment of inertia about the z axis. w_x , w_y and w_z stand for angular velocities about respective axes; T_x , T_y and T_z represent torque acting about the corresponding axis.

$$T_x = I_{zz} w_z w_y . \quad (3.11)$$

The power transmission implies

$$T_y = I_{zz} w_z w_x , \quad \text{so that} \quad T_x w_x = T_y w_y . \quad (3.12)$$

Such relationship can be established by use of a Gyration as shown in Figure 3.10.

The m above the gyration denotes the gyration modulus, where $m = I_{zz} w_z$. This modulus does not have a direction sense associated with it. This modulus is always defined from flow to effort.

$$e_j = m f_i , \quad e_i = m f_j . \quad (3.13)$$

Thus the following expression establishes conservation of power, $e_i f_i = e_j f_j$.

In the electrical domain, an ideal DC motor is represented as a gyrator, where the output torque is proportional to the input current and the back emf is proportional to the motor angular speed. In general, gyrators are used in most of the cases where power from one energy domain is transferred to another, electrical to rotational, electrical to magnetic, and hydraulic to rotational.

The 3-Port junction elements:

The name 3-port [57][70] [71] used for junctions is a misnomer. In fact, junctions can connect two or more bonds. There are only two kinds of junctions, the 1 and the 0 junction. They conserve power and are reversible. They simply represent system topology and hence the underlying layer of junctions, and two-port elements in a complete model is power conserving.

1 junctions have equality of flows and the efforts sum up to zero with the same power orientation. They are also designated by the letter S in some older literature. Such a junction represents a common mass point in a mechanical system, a series connection (with same current flowing in all elements) in an electrical network and a hydraulic pipeline representing flow continuity, etc. A 1 junction with four bonds is shown in Figure 3.11 (One junctions are sometimes indicated by "J").

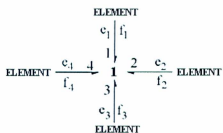


Figure 3.11 Bond graph one junction [70]

Using the inward power sign convention, the constitutive relation (for power conservation at the junction) for Figure 3.11 may be written as follows:

$$e_1 f_1 + e_2 f_2 + e_3 f_3 + e_4 f_4 = 0. \quad (3.14)$$

As 1 junction is a flow equalizing junction,

$$f_1 = f_2 = f_3 = f_4. \quad (3.15)$$

$$\text{Thus, } e_1 - e_2 + e_3 - e_4 = 0. \quad (3.16)$$

So, a 1 junction is governed by the following rules:

The flows on the bonds attached to a 1-junction are equal and the algebraic sum of the efforts is zero. The signs in the algebraic sum are determined by the half-arrow directions in a bond graph.

0 junctions have equality of efforts while the flows sum up to zero, if power orientations are taken positive toward the junction. The junction can also be designated by the letter P. This junction represents a mechanical series, electrical node point and hydraulic pressure distribution point.

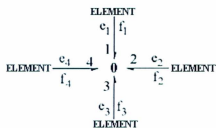


Figure 3.12 Bond graph zero junction [70]

In case of the model above, the constitutive relation becomes,

$$e_1 f_1 + e_2 f_2 + e_3 f_3 + e_4 f_4 = 0. \quad (3.17)$$

as 0 junction is an effort equalizing junction,

$$e_1 = e_2 = e_3 = e_4. \quad (3.18)$$

$$\text{This leads to, } f_1 + f_2 + f_3 + f_4 = 0 \quad (3.19)$$

So, a 0 junction is governed by the following rules:

The efforts on the bonds attached to a 0-junction are equal and the algebraic sum of the flows is zero. The signs in the algebraic sum are determined by the half-arrow directions in a bond graph.

Power directions on the bonds:

Half arrows [70] on the bonds define the direction of positive power flow, and control signals are represented by lines with full arrows. Figure 3.13 shows that when variables are chosen for effort and flow, so that whenever both these variables acquire positive values, the power goes from J to E. However, for mixed signs of the variables, the power direction is reversed.



Figure 3.13 Half arrow: direction of power, E : element, J : junction [70]

Causality:

Causality [70] establishes the cause and effect relationships between the factors of power. In bond graphs, the inputs and the outputs are characterized by the causal stroke. The causal stroke indicates the direction in which the effort signal is directed (by implication, the end of the bond that does not have a causal stroke is the end towards which the flow signal is directed).

To illustrate the basic concept of the causality, let us assume that there is a prime mover with a smart speed governor as shown in Figure 3.14.

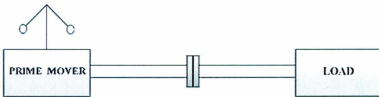


Figure 3.14 Prime mover with a smart speed governor [70]

The prime mover is driving the load (i.e. the power is going from the prime mover to the load). Apart from sending the power, the prime mover also decides that the load should run at a particular speed depending on the setting of the governor. So, it may be said that from the prime mover, the information of flow is generated, which goes to the load. The load generates the information of torque (effort) which the prime mover receives and adjusts the inner mechanisms

to compensate for it. The wavy lines in the following Figure 3.15 indicate the direction of flow of the particular information.



Figure 3.15 Causality between the prime mover and the load [70]

The selected causality is generally indicated by a cross bar or causal bar at the bond end to which the effort receiver is connected. For example sources impose either an effort or a flow but not both, that is why for an effort source there is a causal bar at the end of half arrow and for a flow source the causal bar is next to the flow source and away from a half arrow. For inductance I type storage element, the flow is proportional to the time integral of the effort:

$$\dot{f} = \frac{1}{m} \int e dt \quad (3.20)$$

As an example, a mass subjected to a force that is causing it to accelerate can be considered:

$$v = \frac{1}{m} \int F dt \quad (3.21)$$

For capacitive C type storage elements, the effort is proportional to the time integral of flow:

$$e = k \int f dt \quad (3.22)$$

As an example, a spring being deformed by a force can be considered:

$$F = k \int v dt \quad (3.23)$$

The above integral relationships show that a C element receives flow and generates effort.

The resistive or dissipative elements do not have time integral form of constitutive laws ($e = R.f$ or $f = e/R$)

The flow and the effort at this port are algebraically related and can thus have any type of causal structure, either with an open-ended bond (causal stroke is away from the element, i.e., at the junction end) indicating a resistive causality or a stroke ended bond indicating a conductive causality.

As per the above discussions, the causal strokes for **I**, **C** and **R** elements are shown in the figure below.



Figure 3.16 Causal strokes for C, I and R elements [70]

Sources impose either an effort or a flow on a system, but not both.



Figure 3.17 Causal stroke for effort and flow source [70]

After providing a detailed overview of bond graph methodology, the following section gives a summary on SHD modeling and analysis.

3-2: Sonic Head Drill (SHD) bond graph modeling

Increasing the ROP or drilling rate is one of the main challenges in the drilling industry. ADG has been seeking new technologies and devices to increase the ROP through applying vibratory force to a drill bit. The SHD is used prominently in soil drilling as it generates vibratory force during rotary drilling and increases the ROP. The increase in the ROP in soil drilling has motivated the study of this device for oil and gas drilling. After reviewing several similar technologies, ADG has decided to acquire a SHD for laboratory and field test at Memorial

University. The SHD is used to improve ROP by applying vibratory force to a bit and drill pipe. Several SHDs were analyzed and finally a SHD from Sonic Sampling and Supplies was selected for further analysis and possible purchase. This SHD can produce 100 kN at the maximum frequency of 150 Hz. The SHD uses unbalanced masses to generate sinusoidal forces in the vertical direction along a drill string and a drill bit. The head of the SHD where the vibration is generated, is surrounded by four rubber isolators to reduce the transmission of vibratory force to the drill rig.

The motivation of this study is to determine how much of the generated force is transferred to the rock being drilled and how the output force can be controlled as the head is surrounded by four dampers and the generated force passes through a drill string to get to a bit. That is why an experimental setup was designed to fix one of the rubber isolators on a hydraulic actuator to apply vibratory force and find the relationships between damping and stiffness coefficients with frequency, and then use them in a simulation software along with damping and spring effect of drill string and rock, to analyze the output force of the SHD and evaluate how this force can be controlled at each frequency. ADG has been seeking a range of output forces for laboratory and field tests, and it was required to determine if this device matches the project force profile which is less than 20 kN at the frequency of 100 Hz.

In this analysis, frequencies ranging from 1 to 55 Hz and amplitudes of 0.1 to 2 mm were applied due to hydraulic actuators limitations (higher frequencies and amplitude would shake the machine abruptly). The frame to hold the rubber isolator to the hydraulic actuator was designed in SolidWorks [72] and then manufactured to mount the damper on the hydraulic actuator (Figure 3.18). The force and displacement were recorded at a 1000 Hz sampling rate and then

processed by Matlab [60] to find the spring stiffness and damping coefficient. An Instron 8874 (servo controlled dynamic loading frame) was used for this analysis. This hydraulic actuator has all the sensors required to run this experiment.



Figure 3.18 Rubber isolator mounted on the hydraulic actuator

3-2-1: Computing spring and damper coefficients

A sinusoidal excitation can be used to generate both stiffness and damping parameter values for an element with linear spring and damper properties [73]. The isolator considered in this paper is assumed to behave like a linear spring and viscous damper in parallel, so that

$$F_s = kx \quad (3.24)$$

$$F_d = Cv \quad (3.25)$$

where F_s and F_d are spring and damper force respectively, k is spring stiffness, C is viscous damping coefficient, and x and v are spring/damper endpoint relative displacement and velocity respectively.

For a linear undamped element, the work diagram (plot of force versus displacement) would be a line with stiffness k equal to the slope. The presence of material damping results in a work diagram that has area. The work diagram is assumed to consist of a force component due to stiffness and a force component due to damping. If the spring force F_s is subtracted from the total force F_T and the remaining force is assumed to be the damping force F_d .

Figure 3.19 [74] shows an idealized work diagram from which the stiffness component of total force has been removed to create a work diagram for the damping force only.

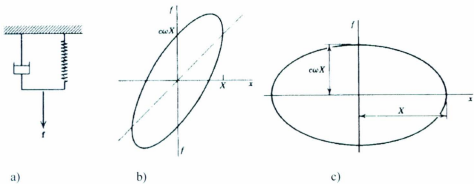


Figure 3.19 a) Schematic; b) Work diagram of total force vs. displacement, showing slope equal to stiffness; c) Work diagram with damping force only [74]

Given the work diagram of Figure 3.19(c), the damping coefficient can be calculated from the area within the curve as follows. In Figure 3.19, ω is the frequency of the vibration and X is the displacement.

Defining work as in equation 3.26:

$$U = \int (f) dx = \int f \left(\frac{dx}{dt} \right) dt \quad (3.26)$$

Differentiating with respect to time and recognizing that the damper is a velocity-based force producing element for which force $f = C \left(\frac{dx}{dt} \right)$, gives the following expression for the time rate of change of work [74]:

$$\frac{dU}{dt} = f \frac{dx}{dt} = C \left(\frac{dx}{dt} \right)^2 \quad (3.27)$$

where C is the damping coefficient.

Integrating, with A representing the area of the work diagram loop,

$$\Delta U = A = \int_0^{2\pi} C \left(\frac{dx}{dt} \right)^2 dt = \int_0^{2\pi} CX^2 \omega \cos^2(\omega t) d(\omega t) \quad (3.28)$$

$$\Delta U = A = \pi C \omega X^2 \quad (3.29)$$

$$C = \frac{A}{\pi \omega X^2} \quad (3.30)$$

The units of work diagram area are (N.m), and the units of the denominator are (m^2/s) , giving overall damping coefficient units (N.s/m) as expected.

When force from an ideal damper is plotted as a function of displacement, we see that the result is indeed an ellipse as shown in Figure 3.19. The equation of the ellipse is derived by substituting into the equation:

$$\sin^2(\omega t) + \cos^2(\omega t) = 1, \quad \left(\frac{x}{X} \right)^2 + \left(\frac{f}{\omega CX} \right)^2 = 1 \quad (3.31)$$

The damping coefficient can also be found more directly using the slope of the damper force versus velocity curve. Generation of this curve again requires that the stiffness component of the total force be removed.

In Section 3-2-2, the damping coefficient is found using both methods. The stiffness k can either be estimated from the slope of the work diagram in Figure 3.19 (b), or from a static test in which the spring/damper unit is moved in small increments to a number of positions, at each of which force is measured after the system comes to rest. Plotting the static test results gives a spring force vs. displacement curve, the slope of which would be stiffness.

3-2-2: Experimental testing and damping and spring coefficients analysis

Table 3.1 gives the experimental test matrix, the extents of which were limited by the hydraulic actuator. At higher amplitudes and frequencies, the hydraulic actuator vibrated to the point where position control was not possible. Force and displacement are recorded by sensors preinstalled on the hydraulic actuator.

Table 3.1 The experimental test matrix

Amplitude (mm)	0.1	0.5	1	2
	Frequency (Hz)			
	1	1	1	1
	5	5	5	5
	10	10	10	10
	15	15	15	15
	20	20	20	20
	25	25	25	25
	30	30	30	30
	35	35	35	
	40	40	40	
	45	45		
	50	50		
	55			

The recorded data for displacement, velocity and force versus time were subtracted by their mean values and then filtered with a high-pass filter. Figure 3.20 shows the effect of calibration and filtering on a sample data set for 20 Hz vibration and 1 mm of displacement amplitude where the first figure is not calibrated and filtered and the second one is. These data sets were then used to generate clean work diagrams of total force, from which the spring stiffness was estimated using the slope (Figure 3.21). The stiffness component of force was then subtracted from total

56

isolator force to find the damping coefficient computed using the slope of the force-velocity curves as well as the area under the work diagram.

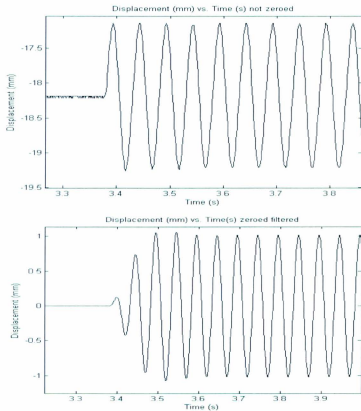


Figure 3.20 Effect of calibration and filtering on 20 Hz vibration at 1 mm amplitude

Figure 3.21 below shows a total force work diagram for 20 Hz frequency and 1 mm displacement. The dashed line in the graph below shows the slope of the force versus displacement which is the spring constant. The slope in Figure 3.21 is 8.78×10^{-4} N/mm.

Once the spring constant is found, it is multiplied by displacement to find the spring force and the spring force is subtracted from the total force to find the force associated with the damping effect.

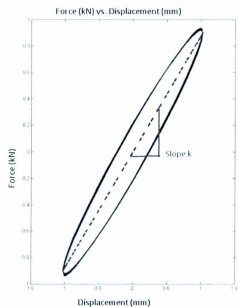


Figure 3.21 Spring constant, the slope of the dashed line

The area of the work diagram (Figure 3.22) and the slope of the damper force versus velocity (Figure 3.23), define the damping coefficient. The damping coefficient using the area of Figure 3.22 is 1.74×10^{-6} N.s/mm.

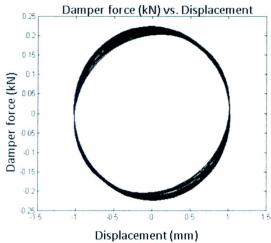


Figure 3.22 Work diagram

Figure 3.23 shows the damper force versus velocity where the slope of the curve defines the damping coefficient which is 1.69 N.s/mm:

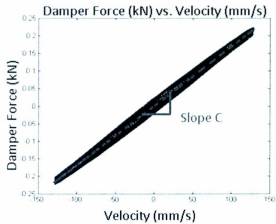


Figure 3.23 Damper force versus velocity

The damping coefficient found using the area of the damper force versus displacement (1.74 N.s/mm) and the slope of damper force versus velocity (1.69 N.s/mm) are sufficiently close with a 2.9% difference.

The spring constants and damping coefficient values found at each frequency and amplitude were then used to create a response surface and regression model to predict stiffness and damping as a function of frequency and amplitude. The response surfaces are shown in Figure 3.24 and 3.25, and the regression equations follow. In these Figures, frequency is in Hz and amplitude is in mm. The points shown in these graphs are the experimental values of spring constant and damping coefficient.

Design-Expert® Software
Factor Coding: Actual
Spring Constant
● Design points above predicted value
■ 1.4751
■ 0.648166
X1 = A: Frequency
X2 = B: Amplitude

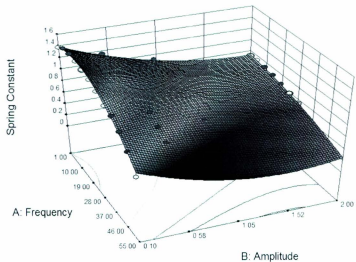


Figure 3.24 Change in the spring constant (kN/mm) with frequency (Hz) and amplitude (mm)

Design Expert® Software
 Factor Coding: Actual
 Original Scale
 Damping Constant
 • Theory points above predicted value
 •

0.00389255
 0.023723

X1 = A: Frequency
 X2 = B: Amplitude

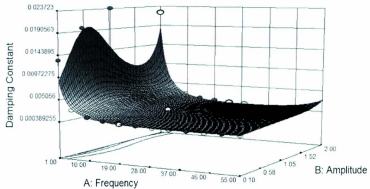


Figure 3.25 Change in the damping coefficient (kN.s/mm) with frequency and amplitude (mm)

The following equations predict the spring constant and damping coefficient at different frequencies (f) up to 55 Hz and amplitude from 0.1 to 2 mm:

$$k = 1.4528 + 0.0134f - 0.7033a - 0.0115f \cdot a - 4.7155 \times 10^{-4}f^2 + 0.1789a^2 + 1.8152 \times 10^{-4}f^2 \cdot a + 1.6345 \times 10^{-3}f \cdot a^2 \quad (3.32)$$

$$1/C_{0.5} = 11.2293 + 1.6583f - 20.0126a - 0.2809f \cdot a - 0.01743f^2 + 19.4964a^2 - 4.0069 \times 10^{-3}f^2 \cdot a - 5.1440a^3 + 4.0591 \times 10^{-3}f^2 \cdot a^2 \quad (3.33)$$

Spring constant depends on both amplitude and frequency. After running preliminary simulations, it was determined that the amplitude of vibration was less than 0.1 mm over the SHD frequency range. Thus, constant amplitude of 0.1 mm was used to create the following equation for spring constant as a function of frequency only:

$$k = 1.3843 + 0.0122f - 4.5340 \times 10^{-4}f^2 \quad (3.34)$$

As shown in Figure 3.25, for frequencies higher than 1 Hz the damping coefficient is only dependent on frequency, so in the dynamic analysis the amplitude is neglected from the equation predicting the damping coefficient and the following equation is used:

$$C^{0.5} = 0.048 + 4.460 \times 10^{-3} \times f - 7.806 \times 10^{-4} \times f^2 + 4.665 \times 10^{-5} \times f^3 - 1.360 \times 10^{-6} \times f^4 + 1.936 \times 10^{-8} \times f^5 - 1.073 \times 10^{-10} \times f^6 \quad (3.35)$$

3-2-3: Dynamic model

A dynamic model was created [6] to study the force transmitted to the frame of the SHD frame and also to the drill string. The parameters found for the isolator spring constant and damping coefficient were used in this model.

The SHD has two unbalanced masses that spin between the frequencies of 1 to 150 Hz. The maximum output force at 150 Hz is 100 kN. The two unbalanced masses generate the force using this formula:

$$F_r = 2m_u r \omega^2 \quad (3.36)$$

where F_r is the vibratory force (total force), m_u is the mass of each unbalanced mass; r is the rotation radius and ω is the angular velocity of the masses. The mass and radius of rotation are constant and the angular velocity is the only parameter that can be modified to change the vibratory force.

The spring constant and damping found in this test were extrapolated to cover the frequencies that were not tested using the hydraulic actuator and then used in the dynamic model to predict the force transmitted to the frame and the drill pipe.

Figure 3.26 shows an outline of the SHD with the rubber isolators, drill pipe, bit and the rock interface. The vertical vibratory force in this system is analyzed by applying the WOB and vibratory force of the SHD at the surface. These parameters are noted in Table 3.2.

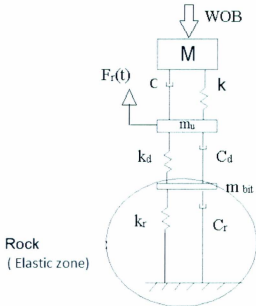


Figure 3.26 System schematic

In the previous diagram M is the mass of the SHD, m_u is the mass of the SHD's core. C and k are the damping and spring constant of the four dampers surrounding the SHD's core. C_d and k_d are the damping and spring constant of the drill string. C_r and k_r are the damping and spring constant of the rock [75]. The frame of the SHD is included in the mass M and the WOB is applied on the frame. The core of the SHD, which included the unbalance masses, is connected to the inside of the frame via the shock absorbers. The WOB can vary up to 55 kN which is the maximum WOB for this SHD.

Table 3.2 The constants and parameters used in the dynamic model

k	Spring constant for the rubber isolator (N/m)	variable
C	Damping coefficient for the rubber isolator (N.s/m)	variable
a	Amplitude (mm)	variable
f	Frequency (Hz)	variable
ω	Rotary speed (rad/s)	variable
F_r	Sonic Head Drill generated force (N)	variable
F_s	Spring force (N)	variable
F_d	Damper force (N)	variable
k_d	Spring constant for the drill pipe (N/m)	3.56×10^9
b_d	Damping coefficient for the drill pipe (N.s/m)	2.163×10^4
k_r	Spring constant for the rock (N/m)	2.23×10^9
b_r	Damping coefficient for the rock (N.s/m)	2.3×10^5
m_{bit}	Inner rod and bit mass (kg)	9.091
m_u	Unbalanced mass (kg)	2.27
WOB	Weight on bit (kN)	20
$W_{sonic\ head}$	Weight of the SHD (N)	4.84×10^4

The dynamic model predicts the following force profile at 150 Hz (Figure 3.28). The SHD generates the force profile at 150 Hz in the second part of Figure 3.28 and the dampers surrounding the SHD, damp out some of the force generated and result in the force transferred to the drill string and eventually the drill bit shown in the third part of Figure 3.28. The force on the frame of the SHD is shown in the first part of Figure 3.28. This force is mainly the weight of the SHD and the WOB. The dynamic fluctuation in this force is attenuated by the dampers to result in a nearly constant value.

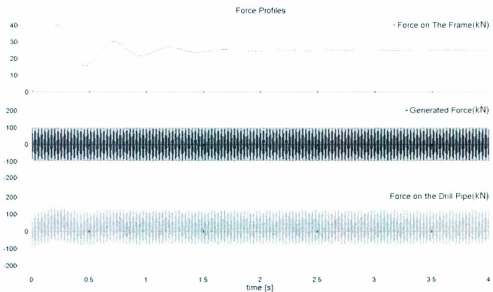


Figure 3.28 Force profile (kN) on the SHD frame, generated force and the force in the drill pipe for $f = 150$ Hz

The force on the frame remains fairly consistent over the entire frequency range of interest due to the presence of the isolators, even as exciting force and frequency increase. Most of the generated force is transferred to the drill string and not the frame. Drilling calculation and

optimization techniques use WOB to predict the ROP and other factors in the drilling process. Having constant static force (which includes WOB), will make the optimization of the drilling process easier. Also, a lot of fluctuation in the static force can damage the equipment at the surface. That is why it is preferred to keep the force on the SHD cover and static force at the surface as constant as possible.

Figure 3.29 shows, for each frequency, the (amplitude of vibration force transmitted to frame) divided by (SHD generated force amplitude). The frequency response function shows a damped resonant peak at approximately 20 Hz, which is expected given the system parameters. Even at the resonance, the dynamic amplitude of transmitted force was only 1.5 % of the generated force amplitude. Much more attenuation is achieved at higher frequencies, which is important given that generated forces increase with the square of frequency.

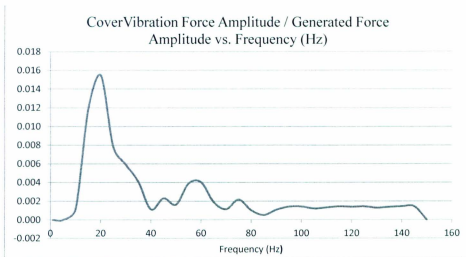


Figure 3.29 Cover force amplitude divided by generated force amplitude

Figure 3.30 shows the ratio of drill string force to generated force. It is important that most of the generated force is transmitted to the drill string for effective drilling. At higher frequencies, the ratio approaches 1, while at lower frequencies dynamic amplification occurs. This is in fact very useful for vibratory drilling; in lower frequencies, lower amount of force is generated and dynamic amplification increases the vibratory force applied to a drill string. At higher frequencies, where the generated force is high, almost all of the force is transferred to the drill string.

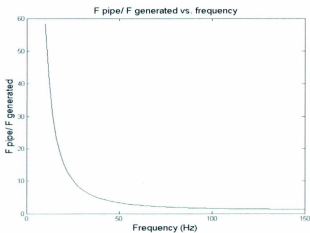


Figure 3.30 Ratio of transmitted force to the drill string and the generated force at each frequency

Figure 3.31 shows the generated force by the SHD at each frequency. One can use Figures 3.30 and 3.31 to get an estimate of the applied force on the drill string.

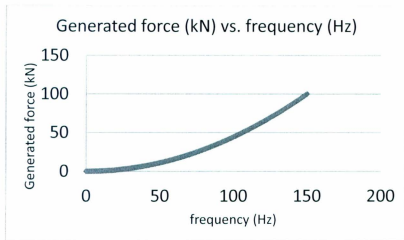


Figure 3.31 Generated force (kN) vs. frequency (Hz)

The simulation results clearly show that most of the generated force is transferred to a drill string with dynamic amplification happening at the lower frequencies. These results are very promising for soil drilling where most of the generated vibratory force is transferred to a drill string and increases the ROP. However, ADG has been seeking a device with lower vibration generated force (less than 20 kN at 100 Hz) and higher control over it for laboratory use purposes. That is why ADG did not purchase this device.

However the concept of rotating unbalanced masses is useful for creating vibratory force and as a result, other devices using this concept were studied and designed to better suite ADG. Section 3.3 discusses an alternative design to create vibratory force for drilling.

3-3: Vibratory System Design

After reviewing several mechanical vibration generation devices, one of them (based on the unbalanced masses concept mentioned before) is selected for further analysis. This design, which was discussed in chapter 2 is based on Longyear Inc. vibratory unit for drilling systems [79]. The design and packaging of this system seem to be very useful for oil and gas drilling. However, it is not clear how much force can be created at the confined space available at the bottom of a well. Figure 3.32 shows the vibration generation device. This device has four gears with two unbalanced masses on each of them. These masses are mounted on each gear in a way that the horizontal components of the generated centrifugal forces cancel each other out, and the vertical components would generate a sinusoidal force along the drill string. The frequency of generated force is controlled by the drilling mud flow rate rotating the gears. It is the purpose of this section to predict the generated force at each frequency and improve the design of this device.

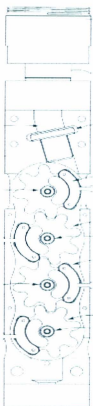


Figure 3.32 Vibratory device for rotary drilling

After the preliminary study on this system, it was determined that if the moment is calculated at the bottom of the tool for each centrifugal force, the summation of moment for each force would not cancel each other out and it would not be zero. This issue can damage the bottom hole equipment, so a modification to this device is proposed. A smaller ideal gear is placed between the upper two and lower gears to cancel the moment generated. Figure 3.33 shows a SolidWorks [72] design based on this patent with the modified design and the ideal gear.

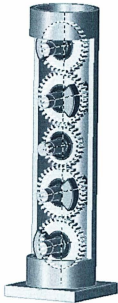


Figure 3.33 Vibration generation device

After running a simulation in SolidWorks for the design shown in Figure 3.33, it became clear that the proposed ideal gear would resolve the moment issue mentioned above.

The system shown in Figure 3.33 uses 8 unbalanced masses that are attached to 4 gears on both sides. It also has an ideal gear in between the top two gears and the bottom two, to cancel the moment.

For the force analysis, a 5 inch (127 mm) diameter is chosen for the vibratory device (different diameters can be selected; changing the diameter would change the total mass and the length of the system). This would give a total mass of 16.46 kg and a length of 0.5 m for the tool (Figure 3.33).

Figure 3.34 shows the properties for the unbalanced mass attached to each gear.



Mass (kg)	Center of mass (m)	Material
0.183	0.0285	AISI 1020

Figure 3.34 Unbalanced mass attached on each gear and its properties

The center of mass is shown with a black dot and is measured from the center.

For devices that are based on the unbalanced mass concept, the generated vibratory force can be calculated using the following equation:

$$F = 8 \times m \times r \times \omega^2 \quad (3.37)$$

Where F is generated force, m (in kilograms) is the mass of the unbalanced part, r (in meters) is the radius from the center of rotation to the center of the mass and ω is the frequency of rotation in revolution per seconds (Hz). The result is multiplied by 8, since there are 8 unbalanced masses in this device.

Figure 3.35 shows a sample simulation result for the force at a frequency of 4 Hz:

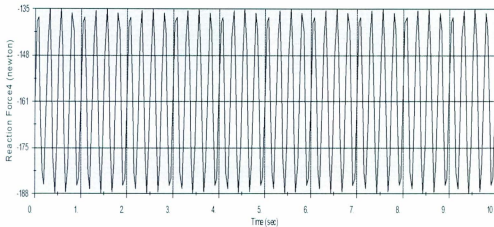


Figure 3.35 Generated force at 4 Hz

The amplitude of the vibratory force generated at 4 Hz is 53 N which is equal to the generated force through equation 3.37. (Generated force through this formula should to be multiplied by two to show the amplitude).

Comparing this system with the SHD, this system can generate 74.5 kN at a frequency of 150 Hz where the SHD generates 100 kN.

The advantage of this system to the SHD is the fact that it doesn't need to be installed at the top of the drill string. This tool can be installed above a drill bit and the generated vibration can be transferred to a bit directly. The rest of the drill string can be isolated from this vibration by using a shock sub. In chapter 4, a sensitivity analysis of shock subs is given. This sensitivity analysis would determine the effect of WOB, damping coefficient, spring coefficient and the location of a shock sub on the axial vibration of a drill string.

The design proposed here has never gone through fabrication; however the SolidWorks models and packaging details are available for further study and fabrication.

Vibration generated by the SHD or any other vibration generation devices is transferred to both a drill bit and a drill string. Although this vibration can be useful in increasing the ROP, when it is transferred to a drill string, it can cause equipment failure or fatigue.

In the next chapter, axial vibration in a drill string will be explained. Axial vibration is an important phenomenon in drilling industry and ways to mitigate this vibration could help protect drilling equipment and avoid drilling failure.

Chapter 4 : Axial Vibration in Drill String

As explained in chapter 2 and 3, axial vibration is an important phenomenon in the drilling industry. In this chapter an overview of axial vibration modeling is explained. This is accomplished by first establishing a drill string model in a commercial simulation software (20Sim [6]) using the bond graph language. In order to build this model and check its validity, two modeling techniques are used in 20Sim to build the drill string model, along with a finite element model (ABAQUS) to compare the first four natural frequencies. Natural frequency is known as the frequencies at which an object tends to vibrate with when hit, struck or somehow disturbed. First natural frequency is defined as the lowest frequency of a periodic waveform [3]. These frequencies are compared for all three models to ensure that they would react almost identically under vibration.

The two modeling techniques used in 20Sim are modal expansion and lumped model. These modeling techniques are explained in section 4-1.

After establishing the 20Sim model, this model is simulated and the results are presented. This model has undergone a force analysis to ensure that it has the same characteristics as an actual drill string.

Later this chapter, the presence of axial vibration in the drill string is presented using the developed drill string model along with a shock sub sensitivity analysis to mitigate this vibration. This axial vibration is generally caused by the bit bounce or rough drilling; however other excitation mechanisms can cause axial vibration too. As an example, the SHD or any similar vibration generation devices can create axial vibration in the drill string. It is the purpose of this

chapter to establish a drill string model for axial vibration study and present a solution in mitigating this vibration.

In order to mitigate the axial vibration in the drill string, section 4-3 will present a sensitivity study on shock sub parameters. In this study, the effect of WOB, damping coefficient, spring coefficient and location of the shock sub from the bit are analyzed and their effects on reducing the axial vibration are detailed. The amplitude of the rotary table vibration is used as a reference to investigate how effective the shock sub is and how these parameters can be tweaked to reduce this vibration.

4-1: Modal expansion, lumped model and finite element model (ABAQUS)

Daniel Bernoulli (1700-1782) developed the notion that string vibrations can be expressed as the superposition of an infinite number of harmonic vibrations. His technique was later developed into a more advanced formulation called modal expansion [86]. In the modal expansion model [57], the system effect at each vibration mode is analyzed and the total effect is the summation of each mode displacement as a function of time. Equation 4.1 shows the general form for the modal expansion where ξ is the summation of displacement at any point and time, Y_n is a function for displacement and η_n is a function of time:

$$\xi(x, t) = \sum_{n=1}^{\infty} Y_n(x) \eta_n(t) \tag{4.1}$$

The advantage of this type of modeling is that the natural frequencies are exact but they must be calculated beforehand and the disadvantage is that it is more difficult to connect other models to any arbitrary points.

Lump segment modeling is the second approach used here to model the drill string. In lumped model analysis, the length of the drill pipe and collar is divided by the number of lumps:

$\Delta x = L/n$ where L is the length of drill pipe or collar and n is the number of lumps selected for an analysis. Δx is then the length of the lump or the small portion that is connect to other parts of the system via compliance element. In this type of analysis, a long beam, drill pipe or collar is divided up to small masses with springs between them. Figure 4.1 shows a drill pipe and collar to the right and a lumped segment model representation of the drill string to the left.

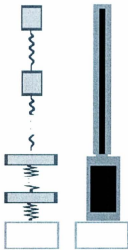


Figure 4.1 Lumped model

As shown in Figure 4.1, the drill pipe and collar are divided up into small masses with springs between them. Δx is a length of each lump or portion. The mass and spring compliance between

each lump are found using equations 4.2 and 4.3, where ρ is a density of a material used for a drill pipe or a drill collar, A is a cross sectional area and E is the modulus of elasticity for the material used in drill pipe or collar:

$$I = \text{mass} = \rho \times A \times \Delta x \quad (4.2)$$

$$C = \text{compliance} = \Delta x / (E \times A) \quad (4.3)$$

The natural frequencies of a lumped segment model converge to the true natural frequencies as the number of lumps increases. In a lumped segment model, it is easy to change the boundary conditions and connect to other models such as rock or the SHD.

ABAQUS is a suite of software applications for finite element analysis and computer-aided engineering [7]. ABAQUS is used in this study to determine the natural frequencies of the drill string and compare them with the other two modeling techniques used in this study.

After providing a short overview of modal expansion, lumped modeling and ABAQUS, they are used to establish the drill string model.

Rather than having the complete drill string model, the drill pipe is analyzed first for the sake of simplicity and the complete drill string model is presented later in this chapter.

A drill pipe model with the length of 5000 m is established using modal expansion, lumped segment model and ABAQUS, and the natural frequencies are compared using these techniques.

Table 4.1 shows the specification for the drill pipe used in this analysis:

Table 4.1 Drill pipe characteristics

Drill pipe	Material	Weight	Nominal diameter	Inside diameter (ID)
	G- 105	20.834 (kg / m)	101.6 (mm)	84.836 (mm)

The material used for the drill pipe is G-105 with a diameter of 84.84 mm (4 inches) and the weight per length of 20.83 kg/cm (14 lbs/ft). The data provided in this table would be used throughout this chapter for the drill pipe analysis.

The boundary condition is fixed at top and free at the bottom for all 3 models.

The Bond Graph below is the modal expansion model of the drill pipe with 5 modes:

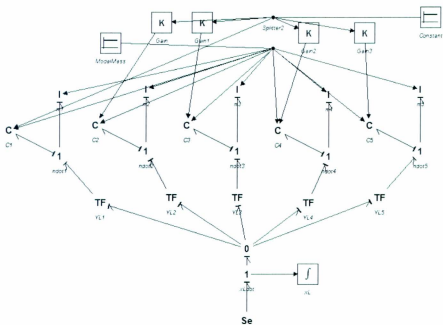


Figure 4.2 Modal expansion model of the drill pipe with 5 modes

In the modal expansion model, the natural frequencies are calculated beforehand. Equation 4.4 [57] shows how w_m is calculated for the modal expansion model where n is the mode number, E is the modulus of elasticity, ρ is the density and L is the length of the drill pipe:

$$w_m = \sqrt{\frac{E(2n-1)\pi}{\rho L} \frac{\pi}{2}} \quad (4.4)$$

For the first mode, the first natural frequency is calculated to be $w_1 = 1.55087$ rad/s. For each inertia element in the bond graph shown in Figure 4.2, the modal mass m_m is calculated using equation 4.5:

$$m_m = \frac{\rho AL}{2} \quad (4.5)$$

After calculating ω and the modal mass, equation 4.6 is used to calculate the spring stiffness for each compliance element C in Figure 4.2.

$$k_m = m_m \omega_m^2 \quad (4.6)$$

$$\omega_1 = 1.55087 \text{ rad/s} \quad k_1 = m_1 \omega_1^2 = 59632.688 \text{ N/m}$$

The rest of the k values are calculated in 20Sim as the natural frequency changes using equation 4.6.

$Y_n(x)$ is the special mode function which in the bond graph shown in Figure 4.2 represents the transformer modulus. It is calculated using equation 4.7 where B_n is a constant and it is assumed to be one for simplicity. For the first five mode shapes, the Y_n values at locations $x=L$ are found below:

$$B_n = 1 \text{ Assumed}$$

$$Y_n(x) = B_n \sin(k_n L \frac{x}{L}) \quad (4.7)$$

$$Y_1 = 5.4831 \times 10^{-3} , Y_2 = 0.0328927 , Y_3 = 0.082154$$

$$Y_4 = 0.152925 , Y_5 = 0.244244$$

After establishing the modal expansion model, the first four natural frequencies are recorded to compare with the lumped segment model and ABAQUS to ensure that all models are having the same response under vibration.

In the next step, a lumped segment model is established. In the lumped segment modeling the drill pipe is divided into small segment or masses with springs or compliance elements between them. For a model with 5 lumps, the length of each lumps segment is 1000 m. Using equation 4.2 and 4.3, the mass of each lump and the spring stiffness for the spring between two lumps is calculated:

$$I = \text{mass} = \rho \times A \times \Delta x = 8487.53 \times 2.45 \times 10^{-3} \times 1000 = 20794.45 \text{ kg} \quad (4.8)$$

$$C = \text{compliance} = \Delta x / (E \times A) = 1000 / (2.07 \times 10^{11} \times 2.45 \times 10^{-3}) = 1.97 \times 10^{-6} \quad (4.9)$$

The values of natural frequencies in this modeling technique converges to true natural frequencies as the number of lumps increases. In this analysis different numbers of lumps are consider to find the optimum number. This is accomplished by comparing the lumped segment models with modal expansion and ABAQUS models. The optimum number is the number of lumps that have almost identical natural frequencies with the modal expansion model and ABAQUS. The optimum number of lumps should also be as small as possible in order to make the analysis faster.

Finally an ABAQUS model of the drill pipe is established by applying the same specification and boundary conditions used in modal expansion and lumped model. Figure 4.3 shows an ABAQUS model with the first mode shape:



Figure 4.3 ABAQUS model (first mode shape)

The first five natural frequencies are recorded for this model and the results are compared with the modal expansion and the lumped models.

Table 4.2 shows the natural frequencies for all models. If the natural frequencies are almost identical, the models should behave similarly under vibration. As mentioned before, different numbers of lumps are considered to find the optimum number for the lumped segment analysis.

Table 4.2 Natural frequencies for different models

Lumped model: No. of Lumps	Natural Frequency (rad/s) 1	Natural Frequency (rad/s) 2	Natural Frequency (rad/s) 3	Natural Frequency (rad/s) 4
2	1.22	3.195		
3	1.318	3.693	5.337	
5	1.405	4.101	6.466	8.306
7	1.445	4.271	6.911	9.249
10	1.476	4.394	7.214	9.873
15	1.5	4.485	7.424	10.29
20	1.513	4.529	7.519	10.46
25	1.52	4.555	7.572	10.56
30	1.525	4.572	7.606	10.62
35	1.529	4.584	7.63	10.66
Modal Expansion	1.548	4.643	7.739	10.83
ABAQUS	1.547	4.642	7.738	10.832

As shown in table 4.2, as the number of lumps increases, the natural frequencies of the lump models converge toward the ones found using modal expansion and ABAQUS.

Figure 4.4 shows how the natural frequencies converge to the same values as the other models as the number of lumps increases. 25 number of lumps were selected for further analysis, since it

has almost the same natural frequencies when compared to the modal expansion model and ABAQUS. Also higher number of lumps were not selected as they can increase the simulation time significantly.

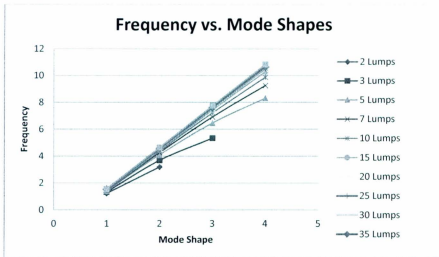


Figure 4.4 Frequency vs. mode shapes for lumped and modal expansion models

In the next step, self-weight is added to all three models to investigate the change in the natural frequencies. In the preliminary analysis, the weight of the drill pipe was neglected in the lumped segment model and ABAQUS for simplify. In order to improve the models in representing the actual drill pipe, self-weight is added to both models. In ABAQUS, it is very easy to add self-weight and it is added through one of the software's option. Adding this option increases the analysis time. Self-weight is added to a lump in the lumped model in Figure 4.5. The figure on the left is taken from 20Sim and it shows how an inertia element is added to the model and the figure on the right shows a schematic of two lumps and how self-weight is added:

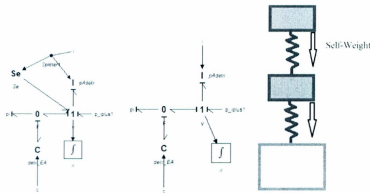


Figure 4.5 Self-weight is added to a lump in a lumped model

After running the simulation models, it became clear that the new natural frequencies were identical to the natural frequency without the self-weight. As mentioned above, it is more realistic to have self-weight in the lumped model and it was expected that the natural frequencies would be the same. The reason is that adding self-weight simply adds a downward force to each lump and does not change the physical behavior of the system. It is known from the vibration theory that self-weight has no effect on the natural frequency, however in order to check the simulation software and the method chosen for this simulation, this analysis was conducted.

The next series of tests are done on the drill string which consists of drill pipe and collar. A 1000 meters drill collar is attached to the analyzed drill pipe. A modal expansion, lumped model and an ABAQUS model is generated to analyze frequency and accuracy of these models. The boundary condition is fixed at top, with free at the bottom.

Table 4.3 shows the specification for the 6 inch drill collar and it will be used throughout chapter 4.

Table 4.3 Drill collar characteristics

Drill Collar	Material	Weight	Nominal Size	Inside diameter (ID)
	G- 105	126.49 kg/m	152.4 mm	57.15 mm

Lumped models with different numbers of lumps for drill pipe and drill collar, and an ABAQUS model were created to compare the natural frequencies. The results are shown in Figure 4.6 (due to high complexity modal expansion model is not developed). Different combinations of lumps are used for drill pipe and drill collar. As an example 25p and 5c represents 25 lumps for the drill pipe and 5 lumps for the drill collar and 25p and 25c represents 25 lumps for the drill pipe and 25 lumps for the drill collar.

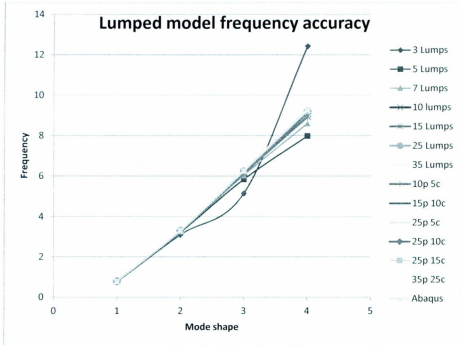


Figure 4.6 Lumped model frequency accuracy for different combinations of lumps

As shown above, as the number of lumps increases the first four natural frequencies for the lump models converges to the values found by ABAQUS. Self-weight was also added to the established models and the results were the identical.

After conducting these analyses, 25 number of lumps were selected as the optimum number for further analysis. The boundary condition used in this section, was selected for the sake of simplicity and to compare the results of the three simulation methods used. In the next section, a new boundary condition is introduced to provide a more realistic condition for the drill string.

4-2: Force analysis in the lumped model

In this section a force analysis for the drill string model is presented. First a drill string model with 25 lumps for both drill pipe and collar is established. The boundary condition for this model is the hook load at the top and fixed at the bottom. Figure 4.7 shows this model:

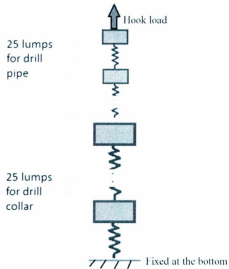


Figure 4.7 Lumped model for the drill string with hook load at the top and fixed at the bottom

A damping element is introduced in this model to take into consideration the effect of the damping of the drill pipe and collar and make the interpretation of the force applied on each lump easier. The equivalent damping factor in the pipe section is about 0.8 lb/ft per sec/ft [52] and 5.0 lb/ft per sec/ft for the collar section.

In addition to the boundary forces, the buoyancy force due to the effect of the drilling fluid is applied on the drill string. Buoyancy is a force exerted by a fluid that opposes an object's weight.

In a column of fluid, pressure increases with depth as a result of the weight of the overlying

fluid. Thus a column of fluid, or an object submerged in the fluid, experiences greater pressure at the bottom of the column than at the top. This difference in pressure results in a net force that tends to accelerate an object upwards. The magnitude of that force is equal to the difference in the pressure between the top and the bottom of the column, and is also equivalent to the weight of the fluid that would otherwise occupy the column. Archimedes' principle is named after Archimedes of Syracuse, who first discovered this law in 212 B.C. (Figure 4.8) [78].

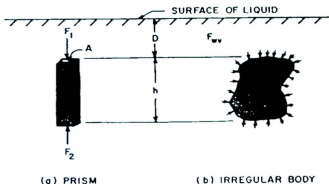


Figure 4.8 Archimedes' principle for objects submerged in fluids [78]

Figure 4.9 shows the effect of drilling hydraulics on the drill string where A_1 is the area of the drill pipe, A_2 is the area of the collar, F_T is the tensile force in the drill string, F_b is the bit force, F_p is the weight of the drill pipe, F_c is the weight of the drill collar, F_1 is the force applied at the top of the collar and F_2 is the force applied at the bottom of the collar.

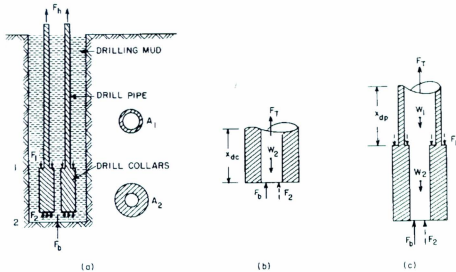


Figure 4.9 Effect of hydraulic pressure on axial forces in drill string; a) Schematic of drill string, b) Free body diagram for drill collars and c) Free body diagram for drill string section [78]

The following analysis shows the forces applied on the drill string at different locations when a drilling fluid with $1.797 \times 10^3 \text{ kg/m}^3$ (15lb/gal) density is used::

$$A_1 = 2.45 \times 10^{-3} \text{ m}^2$$

$$A_2 = 0.015676 \text{ m}^2$$

$$A_2 - A_1 = 0.0132213 \text{ m}^2$$

$$\rho = 15 \text{ (pound / gal)} = 1.797 \times 10^3 \text{ kg / m}^3$$

$$F = \rho g h A \tag{4.10}$$

$$F_1 = 5000 \times 9.81 \times 1797.39641 \times 0.0132213 = 1.166 \times 10^6 \text{ N}$$

$$F_2 = 6000 \times 9.81 \times 1797.39641 \times 0.015676 = 1.658 \times 10^6 \text{ N}$$

$$F_1 = F_p + F_c + F_1 - F_2 = 1.741 \times 10^6 \text{ N}$$

Where F_i is the tensile force in the drill string, which in this case is the hook load at the top of the drill pipe and F_p and F_c are the weights of the pipe and collar section respectively.

Figure 4.10 shows the force versus time for lumps number 9 and 10 which are at 1800 and 2000 meters from the surface. The first 25 lumps are representing the drill pipe and the second 25 lumps in the model represent the drill collar. As shown below these two lumps are in tension.

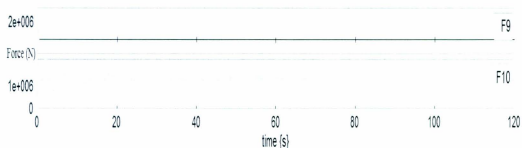


Figure 4.10 Force vs. time for lumps 9 and 10 at 1800 and 2000 meters

The drill pipe is in tension and the drill collar is compressed during a normal drilling process. The drill string in Figure 4.10 is under no excitation force and the decaying vibration in this figure simply shows that the drill string is reaching the equilibrium. Figure 4.11 shows the transition of tension to compression at the depth where the drill pipe and the drill collar are connected.

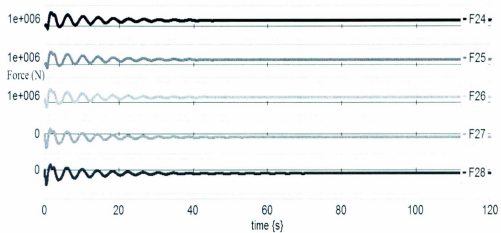


Figure 4.11 Transition of tension to compression between the drill pipe and collar

Force versus axial position for the drill string is shown below (Figure 4.12) where the drill pipe is in tension and the drill collar is in compression. Force versus axial position is commonly used in drilling industry and figure below is used to show that the axial drill string model developed here, has the same characteristics of an actual drill string.

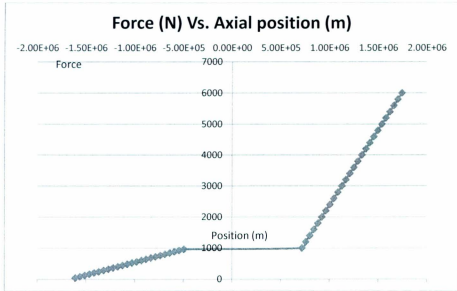


Figure 4.12 Force versus axial position for the drill string

After reviewing the drill data log provided by ADG, a new set of lengths is selected for drill pipe and collar. In the new analysis the drill pipe is 1000 m and drill collar is 200 m. The force analysis for the new lengths of drill pipe and drill collar is shown below:

$$F_1 = 1000 \times 9.81 \times 1797.39641 \times 0.0132213 = 2.33 \times 10^5 \text{ N}$$

$$F_2 = 1200 \times 9.81 \times 1797.39641 \times 0.015676 = 3.317 \times 10^5 \text{ N} \quad (4.11)$$

$$F_t = F_1 = F_p + F_c + F_1 - F_2 = 3.482 \times 10^5 \text{ N}$$

Figure 4.13 shows the force versus axial position for the new length. Once again it shows that the developed model is indeed similar to an actual drill string where that the drill pipe is under tension and drill collar under compression for a normal drilling condition.

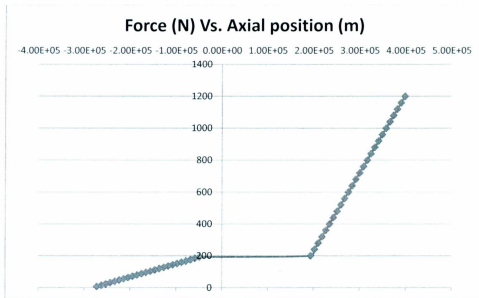


Figure 4.13 Force versus displacement for the drill string

In the next section, axial vibration in the developed drill string model is presented. A sensitivity analysis on shock sub for drilling is conducted to mitigate this vibration.

4-3: Shock sub analysis and study

Shock subs or shock absorbers are used to mitigate vibration in the drill string in the oil and gas drilling. The excess vibration generated due to the use of vibratory tool, bit-rock interaction and drill string wellbore contacts, should be mitigated to increase the ROP and improve the drilling equipment life span. Hence, in this section a sensitivity study on shock sub's parameters and location relative to the drill bit is conducted.

In this section an additional 25 lumps are added to the drill collar for the shock sub sensitivity analysis. This would add up to a total of 50 lumps for the drill collar. The additional 25 lumps would represent the section of the drill collar between the shock sub and the drill bit and the original 25 lumps would represent the section of the drill collar between the drill pipe and the shock sub.

In order to improve the developed model and make it more realistic for the shock sub sensitivity analysis, the bit-rock interaction should also be taken into account. This is accomplished by applying a force with 7 MN amplitude and 45 rad/s frequency at the bottom of the drill collar [52]. Dareing [52] presented the bit rock displacement and this displacement is converted to a force time series to represent the bit-rock interaction.

The existence of the axial vibration in a drill string is shown in the following figures. The drill string model is used to provide an overview of the axial displacement versus time for different sections of the drill string. Figure 4.14 shows the axial displacement versus time for lumps 8 to 10 on the drill pipe.

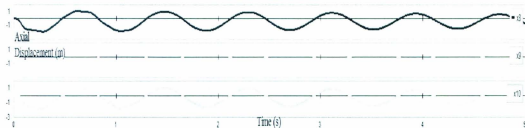


Figure 4.14 Axial displacements vs. time for lumps 8 to 10

Each lump in the drill pipe used in this analysis is 40 m and the figure above shows the lump segments at 280 m to 400 m from the surface. The presence of axial vibration can be clearly seen in this figure.

Figure 4.15 presents the axial vibration versus time for lumps 28 to 30 which are on the drill collar. These lump segments are placed at 1018 m to 1030 m from the earth surface. The presence of axial vibration is again clear on these lumps.

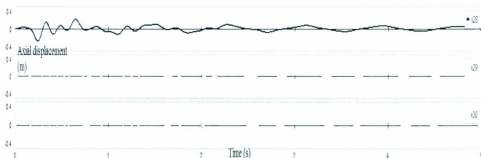


Figure 4.15 Axial displacements vs. time for lumps 28 to 30

Figure 4.16 shows the axial displacement versus time in the last three lumps of the drill collar and once more the axial vibration is present. These lumps are 1194 to 1200 m from the earth surface.

Figures 4.14 to 4.16 present the existence of axial vibration in the drill string at different locations and the purpose of this chapter is to conduct a sensitivity analysis on the shock subs to mitigate this vibration.

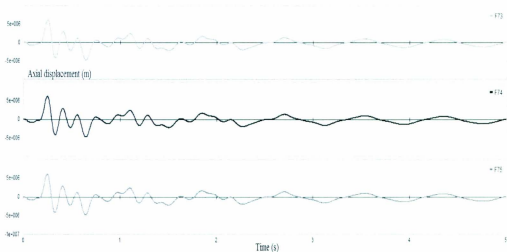


Figure 4.16 Axial displacement vs. time for lumps 73 to 75

Before analyzing the shock sub, another set of figures are presented using the same model by adding the SHD with different frequencies. The purpose of this modification is to analyze the effect of vibratory force on the drill string axial vibration (Figure 4.17).

After running the simulation model by adding the SHD to the axial drill string model, it became clear that the vibratory force only affects the last two lumps at different frequencies. Figure 4.17 shows the axial displacement versus time for the last three lumps on the drill string when the SHD is applying vibratory force at 25 Hz vibration and force output of 2.77 kN. As shown in this figure, SHD only affects the last two lumps and the damping effect of the drill collar and drill pipe mitigate this vibration. The vibration in the other lumps is similar to Figures 4.14 and 4.15. This shows that the generated vibration is not propagated to the surface.

In Figure 4.17 the small vibration with higher frequency is due to the SHD vibratory force at 25 Hz where the axial displacement frequency is about 1.22 Hz.

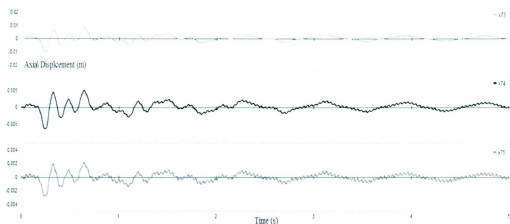


Figure 4.17 Axial displacement vs. time for lumps 73 to 75 with the SHD at 25 Hz

Since the vibratory force by the SHD does not propagate to the rest of the drill string and it only affects the last two lumps, the use of the SHD for shock sub sensitivity study was neglected. The frequency of applied force for the SHD is significantly higher than the natural frequency of the drill string, hence no vibration propagation is observed.

Now that the axial vibration model is established and it is shown in different segment of the drill string, the following analysis would find the optimum parameters for the shock sub to mitigate the vibration.

The shock sub used in this analysis is an active damper consisting of a damper and spring and it is the purpose of this study to find the optimum WOB, location of the shock sub from the bit and the shock sub damping and spring coefficient, in order to mitigate the axial vibration. In this sensitivity analysis, the surface axial vibration amplitude is used as a reference to study the shock sub effectiveness and how shock sub parameters are affecting this amplitude. Table 4.4 shows the range of these parameters. The shock sub parameters range (B and C) and location were

selected from APS Technology [87] and the WOB range used in this analysis are selected by the ADG WOB criteria.

Table 4.4 Shock sub analysis parameters

WOB (kN)	50	200
B (N.s/m)	87563.5	437817.5
C (m/N)	4.76E-008	9.52E-08
location (m)	2	10

Using the parameters presented in this table, a test matrix is established in Design Expert software [5]. A response surface method (RSM) is used in this analysis which helps determine the relationships between one or more measured responses and the vital input factors. To reduce the number of runs, a Central Composite Design (CCD) is applied. CCD is the most popular RSM design, which is used to estimate the coefficients of a quadratic model to fit to a surface generated by this analysis. Thirty runs are chosen by Design Expert to estimate the effect of these four parameters.

Table 4.5 shows the first four runs and the result for each simulation.

Table 4.5 Sample test runs

Run	Factor 1 A:WOB (kN)	Factor 2 B:B (N.s/m)	Factor 3 C:C (N/m)	Factor 4 D:L (m)	Response 1 Rotary Table X m
1	125.00	262690.50	7.14E-08	6.00	0.1801
2	125.00	262690.50	7.14E-08	6.00	0.1801
3	125.00	262690.50	7.14E-08	2.00	0.1705
4	87.50	350254.00	8.33E-08	8.00	0.1528

After analyzing the data for these runs, the results show that the amplitude of axial displacement at the surface is mostly dependent on WOB, damping coefficient, and spring coefficient respectively and the location of the shock sub has a small effect on this amplitude. Equation 4.9 shows how the rotary table amplitude is calculated using these parameters:

$$\text{Rotary Table X (m)} = +0.518 - 1.085 \times 10^{-3} \times \text{WOB (kN)} - 2.717 \times 10^{-7} \times \text{B (N.s/m)} - 1.921 \times 10^6 \times \text{C (N/m)} + 1.605 \times 10^{-4} \times \text{L (m)} \quad (4.9)$$

In statistics, the coefficient of determination R^2 is used in the context of statistical models whose main purpose is the prediction of future outcomes on the basis of other related information. It is the proportion of variability in a data set that is accounted for by the statistical model [88]. R^2 provides a measure of how well future outcomes are likely to be predicted by the model. In this model R-squared is 0.9752 which shows the high level of accuracy for the predicted values using the generated model (a model will be more accurate as this value converges to unity). It also means that the 3D surface plots shown below are almost perfectly fitted around the data points.

Figure 4.18 shows how the amplitude of the rotary table changes as the damping constant and WOB varies. Increasing the WOB can effectively reduce the rotary table vibration and if increasing the WOB is not enough or is not possible due to drilling constraints, a shock sub with higher damping constant can be used to reduce this amplitude.

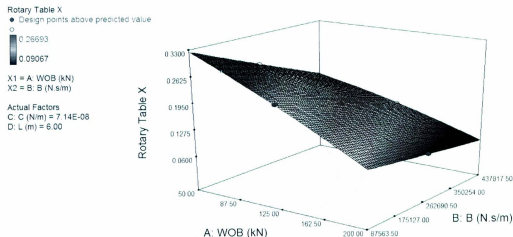


Figure 4.18 Rotary table displacement amplitude vs. WOB and damping coefficient

Figure 4.19 shows how the amplitude of the rotary table changes by varying WOB and spring coefficient for the shock sub. Increasing the WOB would reduce the rotary table amplitude, same as increasing the spring coefficient. However increasing the spring coefficient is not as effective as the damping constant and WOB. This could be seen from Figure 4.20 where the slope of the line representing the damping coefficient is higher than the slope of the line representing C. This graph is generated when the WOB is at 125 kN and the shock sub is located at 6 m from the bit (similar results were generated by varying the WOB and the location of the shock sub).

Design-Expert® Software

Rotary Table X

● Design points above predicted value



X1 = A: WOB (kN)
X2 = C: C (N/m)

Actual Factors

B: B (N.s/m) = 262690.50
D: L (m) = 6.00

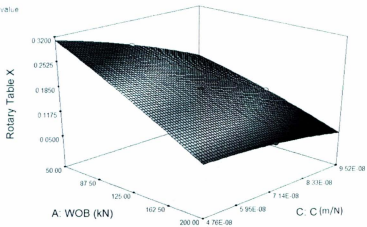


Figure 4.19 Rotary table displacement amplitude vs. WOB and spring coefficient

Design-Expert® Software
Factor Coding Actual
Rotary Table X
— CI Bands

X1 = B: B (N.s/m)
X2 = C: C (N/m)

Actual Factors
A: WOB (kN) = 125.00
D: L (m) = 6.00

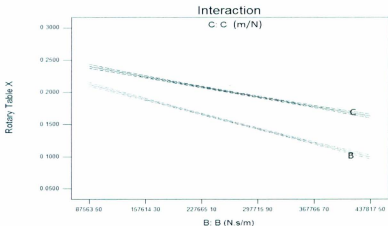


Figure 4.20 Damping and spring coefficient interaction

Figure 4.21 shows the effect of WOB and location of the shock sub on the amplitude of rotary table vibration. As it is shown the location has the lowest effect on this amplitude.

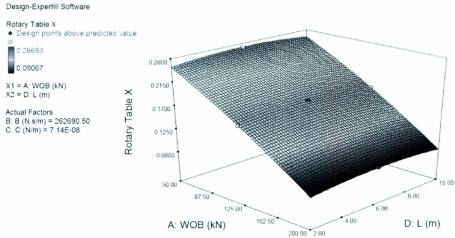


Figure 4.21 Rotary table displacement amplitude vs. WOB and location of the shock sub

Figure 4.22 shows the effect of damping and spring coefficient on the amplitude of the rotary table. As it is shown below increasing the damping and spring coefficient would decrease the amplitude of vibration for the rotary table with damping coefficient having a slightly higher effect. One could argue that it is known that increasing the damping and spring coefficient of the shock sub would reduce the vibration amplitude, however this sensitivity analysis provide a detail overview on how much these two parameters should change in order to reduce the rotary table amplitude.

Design-Expert® Software

Rotary Table X

● Design points above predicted value

○

0.26693

0.09067

X1 = B (N.s/m)

X2 = C (N/m)

Actual Factors

A. WOB (kN) = 125.00

D. L (m) = 6.00

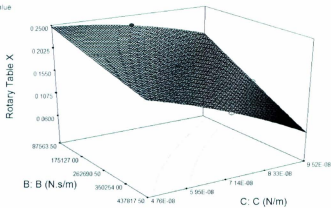


Figure 4.22 Rotary table displacement amplitude vs. damping and spring coefficient

In this section, a sensitivity study on a shock sub was presented to find the optimum parameters for a shock sub to reduce the amplitude of vibration of a rotary table. The results show that WOB and damping constant have the highest effect on reducing the amplitude. These parameters can be used to design and utilize a shock sub for laboratory tests and field drilling.

The drill string model developed in this chapter can also be used for further studies and analysis and can be used with different boundary conditions, drilling tools and percussive or vibration generation devices. This model can also be further developed to incorporate torsional and lateral vibrations.

Chapter 5 : Concluding Remarks and future work

This study presented an overview on vibration generation devices for rotary drilling with an emphasis on the SHD and also including the effect of axial vibration on a drill string.

ADG has been seeking new technologies to improve the ROP and also enhance drilling operation and reduce drilling failure. In this regard a review of rotary drilling, percussive rotary drilling, application of vibration in rotary drilling and other innovative techniques were presented in chapter 2. The main focus in this study is on the application of vibratory force on rotary drilling and its effect on axial vibration. Several vibration generation systems were detailed and one of the prominently used vibration generation devices were selected for further study. ADG has been seeking to acquire drilling equipment for laboratory and field tests, and the SHD as one of the prominently used drilling tools in soil drilling, was selected for further analysis and possible purchase. The vibratory force of this device is generated by two unbalanced masses that rotate in opposite directions, generating centrifugal forces where the horizontal components of these forces cancel each other out and their vertical forces components are added to WOB, acting as a vibratory force. The SHD is surrounded by four dampers to reduce the vibration transferred to the drilling frame, and transfer most of the generated force to a drill string and eventually to a bit. It was not clear however, how these dampers are affecting the generated force. In chapter 3, a series of tests were presented in which a hydraulic actuator was used to test an isolator or a damper surrounding the SHD's core, to determine the change of damping and spring constant with frequency. The results were presented in chapter 3 and equations were generated to predict how these parameters vary with frequency. These equations were then used in a 20Sim model to predict the output force and the force transferred to a drill frame. It is worth noting that Bond

107

Graph modeling was used for the computer simulation analysis and the basics of Bond Graph are detailed in this chapter. The simulation results showed that most of the force generated is transferred to a drill string with dynamic amplification for lower frequencies. The generated vibratory force however was not transferred to the drilling frame, and the only force on the drilling frame was the WOB and the weight of other component used in drilling. Although these results sound promising and show the effectiveness of the isolators, the generated force by SHD was beyond need of ADG and the focus of this group has shifted to different technologies.

In future work, the damper can be tested in the laboratory at various non-zero static deflections to expand the spring-damper equation model. Also increasing the complexity and fidelity of the rock model would be the next step towards creating a predictive simulation environment to assess the effect of vibration force on drilling effectiveness.

Although SHD was not acquired by ADG, the concept of unbalanced masses seemed to be a very promising method in generating vibratory force. This concept is further studied in chapter 3 and a design to generate vibratory force was presented. The output force of the proposed design is lower than SHD. At 4 Hz this device can generate 53 N and at 150 Hz this device is capable of generating 74.5 kN comparing to 100 kN for the SHD. This design can be further analyzed and it could be refined for prototyping and laboratory tests.

Bit rock interaction, vibration generation devices and other factors can create axial vibration in a drill string which can cause drilling equipment failure, fatigue and decrease in the drilling efficiency. In chapter 4, an investigation on axial vibration is presented. In this study an overview of axial vibration in the drill string, along with methods of mitigating this vibration is presented. In this study, three drill string models were created and these models were compared

to study the accuracy and ease of use. Lumped modeling was eventually selected to continue the drill string analysis as it is very easy to implement and changing the boundary condition is not as tedious as the other two methods. Force analysis for this model was presented and it was shown that the drill pipe was in tension and drill collar was in compression as it should be during a conventional drilling operation. The same analysis was also done when a SHD is generating vibration and it was shown that the force versus depth for the drill string would change slightly and the generated vibration would not propagate to the surface.

In order to reduce the axial vibration, a method of mitigating axial vibration is explained in this chapter. A sensitivity analysis on a shock sub is presented. In this analysis the effect on WOB, shock sub damping coefficient, shock sub spring coefficient and shock sub location on the amplitude of rotary table vibration is presented. It is shown that WOB, damping and spring coefficients have strong effects on this amplitude and increasing them could reduce the rotary table amplitude.

In future work, the lumped model presented in chapter 4 can be modified to accommodate the lateral and torsional vibration. Rock model used in this analysis could also be further studied and the model can be further modified to predict the ROP. The effect of resonance on drilling can also be studied and the shock sub model studied in this chapter can be used to mitigate the vibration generated from being transferred to other parts of the drill string. The model of drill string generated can be used in other drilling analysis as the lumped model can be easily integrated to other models. The effect of underbalanced drilling could also be studied by reducing the WOB in the drill string model. Furthermore, different lengths for drill pipe and collar can be used to widen the range of the drill string lengths.

References

- [1] Jardine, S., Malone, D., and Sheppard, M., (1994), *Putting a Damper on Drilling's Bad Vibrations*. Oilfield Review, January 1994
- [2] Hayes, M. (2009), *Shocks and Vibrations: a cause of drill string failure*, Schlumberger productive drilling.
- [3] Rao, S. S., (2009), *Mechanical Vibrations*, fifth edition, Pearson.
- [4] Bruce, D., (2006), *The basics of geotechnical construction drilling*, National Drillers Article, March.
- [5] Design Expert 8.0.1, Stat-Ease Inc., Minneapolis, MN, 2010
- [6] 20sim v.4.1, (2010) Controllab Products b.v., Enschede, Netherlands.
- [7] ABAQUS 6.10, (2010) Dassault Systems, Concord, MA.
- [8] Daqing, H. C., Tie, Y.,(2009), *The research on axial vibration of drill string with Delphi*, Petroleum Engineering Institute, Heilongjiang, China.
- [9] Fernandez, J. V., Pixton, D. S., (2005) Integrated drilling system using mud actuated down hole hammer as primary engine, Novatek, December 2005
- [10] Tibbitts, G., Judzis, A., (2003) Optimization of mud hammer drilling performance, A program to benchmark the viability of advanced mud hammer drilling, TerraTek, January
- [11] Bodine, A. G., (1972). *Sonic drilling device*, US patent 3684037, August 1972
- [12] Kestner, P., (2001) *Sonic drilling catalog*, Boart LongYear, October, 2001
- [13] Wiercigroch, M. (2008). Vibrational energy transfer via modulated impacts for percussive drilling. *Journal of theoretical and applied mechanics*, vol. 46(3), 715-726.

- [14] Han, G. (2006). *Percussion drilling: From laboratory tests to dynamic modeling*. SPE international oil and gas conference, China.
- [15] Bailey, J. R. (2008). *Development and application of BHA vibrations model*. International petroleum technology conference (IPTC), Malaysia.
- [16] Elsayed, M. A. (2005). *Modeling of drill strings*. 24th ASME international conference on offshore mechanics and arctic engineering (OMAE), Greece.
- [17] Spanos, P. D. (1992). Advances in dynamic bottomhole assembly modeling and dynamic response determination. IADC/SPE Drilling conference, U.S.A.
- [18] Spanos, P. D. (1997). Bottomhole assembly modeling and dynamic response determination. *Journal of energy resources technology*, vol. 119, 153-157.
- [19] Melakhessou, H. (2002). *Nonlinear model for dynamic behavior of drill string*. ASME engineering technology conference on energy (ETCE), U.S.A.
- [20] Navarro-Lopez, E. M. (2007). Avoiding harmful oscillations in a drill string through dynamical analysis. *Journal of sound and vibration*, vol. 307, 152-171.
- [21] Khulief, Y. A. (2009). Laboratory investigation of drill string vibrations. *Journal of mechanical engineering science (ImechE)*, vol. 223, 2249-2262.
- [22] Khulief, Y. A. (2007). *Experimentally-tuned mathematical model for drill string vibrations*. ASME International design engineering technical conference (IDETC/CIE), U.S.A.
- [23] Raymond, D. W. (2007). *Laboratory simulation of drill bit dynamics using a model-based servo-hydraulic controller*. 26th ASME international conference on offshore mechanics and arctic engineering (OMAE), U.S.A.

- [24] Franca, L. F. P. (2003). *Experimental and numerical study of a new percussive drilling model with a drift*. ASME International design engineering technical conference (IDETC/CIE), U.S.A.
- [25] Jogi, P. N. (2002). *Field verification of a model-derived natural frequencies of a drill string*. ASME energy sources technology conference, U.S.A.
- [26] Bourgoyne, A. T. (1986). *Applied drilling engineering*. Texas: society of petroleum engineers (SPE).
- [27] Darcing, D. W. (1984b). *Guidelines for controlling drill string vibrations*. Energy sources conference, ASME, Texas, USA.
- [28] Hakimi, H. (2009). Drill string vibration analysis using differential quadrature method. *Journal of petroleum science and engineering*, vol. 70, 235-242.
- [29] Jackson, W. E. (2000). *Making hole*. PETEX 2000.
- [30] Leine, R. I. (2002). *Stick-slip whirl interaction in drill string dynamics*. Journal of vibration and acoustics, vol. 124, 209-220.
- [31] Zifeng, L. (2007). *Analysis of longitudinal vibration of drill string in air and gas drilling*. SPE rocky mountain oil & gas technology symposium, U.S.A.
- [32] Aminfar, O. (2008). *Torsional vibration analysis of drill string in blast hole drilling*. ASME international mechanical engineering congress (IMECE), U.S.A.
- [33] Heisig, G. (2000). *Lateral drill string vibrations in extended-reach wells*. IADC/SPE Drilling conference, U.S.A.
- [34] Christoforou, A. P. (2001). *Active control of stick-slip vibrations: The role of fully coupled dynamics*. SPE middle east oil show, Bahrain.

- [35] Al-Hiddabi, S. A. (2003). Nonlinear control of Torsional and bending vibrations of oil well drill strings. *Journal of sound and vibration*, vol. 265, 401-415.
- [36] Yigit, A. S. (1998). Coupled Torsional and bending vibrations of drill strings subject to impact with friction. *Journal of sound and vibration*, vol. 215 (1), 167-181.
- [37] Yigit, A. S. (2000). Coupled Torsional and bending vibrations of actively controlled drill strings. *Journal of sound and vibration*, vol. 234 (1), 67-83.
- [38] Khulief, Y. A. (2005). Finite element dynamic analysis of drill strings. *Journal of finite element in analysis and design*, vol. 41, 1270-1288.
- [39] Yigit, A. S. (1996). Coupled axial and transverse vibrations of oil well drill strings. *Journal of sound and vibration*, vol. 195 (4), 617-627.
- [40] Sampaio, R. (2007). Coupled axial Torsional vibrations of drill strings by means of nonlinear model. *Journal of mechanics research communications*, vol. 34, 497-502.
- [41] Elsayed, M. A. (2002). Analysis of coupling between axial and Torsional vibration in a compliant model of a drill string equipped with a PDC bit. ASME engineering technology conference on energy (ETCE), U.S.A.
- [42] Leine, R. I. (2002). Stick-slip whirl interaction in drill string dynamics. *Journal of vibration and acoustics*, vol. 124, 209-220.
- [43] Challamel, N. (2000). A stick-slip analysis based on rock-bit interaction: theoretical and experimental contribution. IADC/SPE Drilling conference, U.S.A.
- [44] Baumgart, A. (2000). Stick-slip and bit-bounce of deep-hole drill strings. *Journal of energy resources technology*, vol. 122, 78-82.

- [45] Yigit, A. S. (2006). Stick-slip and bit-bounce interaction in oil well drill strings. *Journal of energy resources technology*, vol. 128, 268-274.
- [46] Jardine, S. (1994). Putting a damper on drillings bad vibration. *Oilfield review*, vol. 12, 15-20.
- [47] Ashley, D. K. (2001). *Extending BHA life with multi vibration measurements*. IADC/SPE drilling conference, Texas, USA.
- [48] Shuttleworth, N. E. (1998). Revised drilling practices, VSS-MWD tool successfully addresses catastrophic bit/drill string vibration. IADC/SPE drilling conference, Texas, USA.
- [49] Kreisle, L. F. (1970). Mathematical analysis of effect of shock sub on the longitudinal vibrations of an oil well drill string. *Society of Petroleum Engineers Journal*, vol. 10, No. 4, 349-356.
- [50] Bailey, J (1960). An analytical study of drill string vibration." *Journal of Engineering for Industry, Transaction of the ASME*, vol. 82, No.2, 122-128.
- [51] Paslay, P. (1963). Drill string vibrations due to intermittent contact of bit teeth. *Journal of Engineering for Industry, Transactions of the ASME*, 85, No.2.
- [52] Dareing, D. W. (1968). Longitudinal and angular drill string vibrations with damping. *Journal of Engineering for Industry, Transaction of the ASME*, vol. 90, No.1, 54-61.
- [53] Kreisle, L. F. (1970). Mathematical analysis of effect of shock sub on the longitudinal vibrations of an oil well drill string. *Society of Petroleum Engineers Journal*, vol. 10, No. 4, 349-356.
- [54] Spanos, P. (1995). Modeling of roller cone bit lift-off dynamics in rotary drilling. *Journal of Energy Resources Technology*, vol. 117(2), 115-124.

- [55] Dareing, D. (1984 a). Drill collar length is a major factor in vibration control. *Journal of Petroleum Technology*, vol. 36, No.4, 637-644.
- [56] Chin, W. C. (1994). *Wave propagation in petroleum engineering*. Texas: Gulf publishing company.
- [57] Karnopp, D. C. (2006). *System Dynamics: Modeling and Simulation of Mechatronic Systems* (4th edition). New Jersey: John Wiley & Sons, Inc.,
- [58] Clayer, F. (1990). The effect of surface and downhole boundary conditions on the vibration of drill strings. 65th annual SPE conference, New Orleans, USA.
- [59] Elsayed, M. A. (2006). *Analysis of shock absorber characteristics for drill strings*. 8th biennial ASME/ESDA conference, Torino, Italy.
- [60] Matlab Simulink[®] v.2010, The Mathworks Inc., Natick, MA.
- [61] Chen, D.C.K., Oster, J.H., Sinor, L.A., Warren, T.M. (1998) *Shock Sub Performance Tests*. IADC/SPE Drilling Conference.
- [62] Eskin, M., Leviant, A., Maurer, W.C., (1995) *Former-USSR R&D on Novel Drilling Techniques*. Maurer Engineering Inc.
- [63] Halsey, G.W., Kylling, A., Kyllingstad, A. (1988). *Torque Feedback Used to Cure Slip-Stick Motion*. SPE 18049.
- [64] Tucker, R.W., Wang, C. (Jan 1999) *On the Effective Control of Torsional Vibrations in Drilling Systems*. Department of Physics, Lancaster University.
- [65] Craig, P.G., Worford, S.W., (1983) *Shock Absorbers – Are They Necessary?* IADC/SPE 11406.

- [66] Jansen, Johan D., Stulemeijer, IVO P.J.M., Van Walstijn, Bartholomeus G.G., Worrall, Robert N., (June 1992) *Method and System for Controlling Vibrations in Borehole Equipment*. U.S. Patent No. 5,117,926. Retrieved Aug. 13, 2010 from Google Patents.
- [67] Barbely, Jason A., Burgess, Daniel E., Cobern, Martin E., Perry, Carl A., Was-sell, Mark E., (2007) *Drilling Tests of an Active Vibration Damper*. SPE/IADC Drilling Conference.
- [68] Bakenov, A.S., Gabler, T., Detournay, E., Germy, C.,(2003) *Enhanced drilling performance through drill string vibrations*, AADE Conference, Texas.
- [69] Wiercigroch, M., Akisanya, A., Aphale, S. (2010) *Resonance enhanced Drilling*, ITI Energy Ltd.
- [70] Wolfgang, B.,(2004), *Bond graph methodology*, Springer, Germany
- [71] Breedveld, P., (2003), *Bond graphs- Physical systems modeling 1: Fundamental concepts*, University of Twente, Netherlands.
- [72] SolidWorks v.2010. Dassault Systemes SolidWorks Corp, Concord, MA.
- [73] Rideout, D.G. (1998) *Dynamic Testing and Modeling of the Interconnected Hydragas Suspension System*, M.A.Sc. Thesis, Queen's University, Kingston, ON.
- [74] Steidel, R.F. (1989) *An Introduction to Mechanical Vibrations*, 3 Ed., John Wiley and Sons.
- [75] Sazidy, M. S., Rideout, D.G., Butt, S.D., Arvani, F. (2010) *Modeling Percussive Drilling Performance using Simulated Visco-Elasto-Plastic Rock Medium*, Proc. ARMA Annual Conference, Salt Lake City, USA, 2010.
- [76] Ibrahim, G., Drenth, C. L., Lachance, L. (2008) *Vibratory unit for drilling systems*, US Patent 2009/0173542 A1, Longyear.
- [77] Kolle, J., (2004) *Hydraulic Pulse Drilling*, Tempress Technologies Inc., Kent, WA.

- [78] Bourgoyne, A.T., Millheim, K.K., Chenevert, M.E., Young Jr., F.S., (1986) *Applied drilling engineering*, SPE.
- [79] Smith, F. W. (1961). *Oilfield percussion drilling*. SPE California regional meeting, Bakersfield, California, USA.
- [80] Samuel, G. R. (1996). *Percussion drilling ... Is it a lost technique? A review*. Permian oil and gas recovery conference, Texas, USA.
- [81] Han, G. (1999). Technology assessment for fundamental research on percussion drilling: Improved rock mechanics analysis, advanced simulation technologies full scale laboratory investigation. Report submitted to U.S. department of energy- Contract No. DE-FC26-03NT4.
- [82] Han, G. (2005). *Percussion drilling in oil industry: Review and rock failure modeling*. National technical conference and exhibition for American association of drilling Engineers (AADE), Texas, USA.
- [83] Bates, R. E. (1964). *Field results of percussion air drilling*. 39th SPE annual fall meeting, Texas, USA.
- [84] Melamed, Y. (2000). *Hydraulic hammer drilling technology: Developments and capabilities*, Journal of energy resources technology, vol. 122), 1-7.
- [85] Kutzner, C. (1996). *Grouting of Rock and Soil*, A.A. Balkema, Rotterdam, Netherlands.
- [86] Darrigol, O. (2007) *The acoustic origins of harmonic analysis.* Archive for History of the Exact Sciences, vol. 61.
- [87] Cobern, M., Wassell M. E., (2005) *Laboratory testing of an activedrilling vibration monitoring and control system*, APS Technology, Inc.

[88] Steel, R. G. D. and Torrie, J. H., (1960). *Principles and Procedures of Statistics*, New York: McGraw-Hill.



